Universidade de Aveiro Departamento de Electrónica, Telecomunicações e Informática,
2016

Rui Miguel Fernandes Caseiro

Avaliação do Desempenho de um Sistema de Comunicações Híbrido na Banda das Ondas Milimétricas com Informação Limitada

Performance Evaluation of Hybrid Millimeter Wave Systems Under Limited Information

Rui Miguel
Fernandes Caseiro

Avaliação do Desempenho de um Sistema de Comunicações Híbrido na Banda das Ondas Milimétricas com Informação Limitada

Performance Evaluation of Hybrid Millimeter Wave Systems Under Limited Information

Dissertação apresentada à Universidade de Aveiro para cumprimento dos requesitos necessários à obtenção do grau de Mestre em Engenharia Eletrónica e Telecomunicações, realizada sob a orientação científica do Professor Doutor Adão Silva (orientador), Professor auxiliar do Departamento de Eletrónica, Telecomunicações e Informática da Universidade de Aveiro e da Doutora Sara Teodoro (co-orientadora), investigadora no Instituto de Telecomunicações de Aveiro.

o júri / the jury

presidente / president

Professor Doutor António José Nunes Navarro Rodrigues
Professor Auxiliar, Universidade de Aveiro

vogais / examiners committee

Doutor Paulo Jorge Coelho Marques
Professor Adjunto, Instituto Politécnico de Castelo Branco (Arguente Principal)

Professor Doutor Adão Paulo Soares da Silva
Professor Auxiliar, Universidade de Aveiro (Orientador)

agradecimentos / acknowledgements

Em primeiro lugar, a toda a minha família, por todo o apoio, mas principalmente aos meus pais pela oportunidade que me deram de hoje estar onde estou, e esforço que fizeram por mim.

Agradecer ao meu orientador, Professor Doutor Adão Silva, e à minha coorientadora, Doutora Sara Teodoro, pela sua ajuda, paciência, supervisão e total disponibilidade.

A todos os docentes pelos ensinamentos transmitidos, não só para o desenvolvimento académico, mas também pessoal.

Por último, agradecer a todos os colegas e amigos que me acompanharam ao longo destes anos, por toda amizade e companheirismo.

Palavras Chave 5G, ondas milimétricas, MIMO massivo, quantização de canal

Resumo

O aumento de dispositivos eletrónicos sem fios, acaba por apresentar problemas face às arquitecturas atuais. A atual arquitectura 4G não consegue suportar as exigencias que advêm do aumento de utilizadores e irá portanto ser necessário lidar com maior tráfego e ligações com uma maior taxa de transmissão. Consequentemente, para atender a esses requisitos, novas tecnologias e técnicas são necessárias para a próxima geração (5G).

Técnicas como o uso de ondas milimétricas combinadas com terminais equipados com grandes agregados de antenas ou número massivo de antenas, embora promissoras e apresentando bons resultados, trazem novos problemas. O uso de ondas milimétricas devido ao menor comprimento de onda, permitirão equipar os terminais com um número elevado de antenas. Foi proposto um novo processamento de sinal de transmissão e recepção (por exemplo, beamforming híbrido) para comunicações de ondas milimétricas combinadas com um número massivo de antenas. Contudo, beamforming de transmissão requer o conhecimento da informação de estado do canal antes da transmissão. Portanto, o projeto de técnicas de feedback eficientes é de grande importância para sistemas práticos. Este problema é mais relevante para sistemas baseados em MIMO massivo, uma vez que a informação do canal que é necessária enviar do receptor para o transmissor é muito maior que os sistemas MIMO convencionais.

Nesta dissertação é proposto um método de quantização de canal eficiente que exige uma ligação de baixo débito do recetor para o transmissor. Em seguida, é avaliado um sistema mmW mMIMO de utilizador único sob a estratégia de quantização desenvolvida. Foi considerado um transmissor possuíndo um equalizador híbrido analógico-digital. As técnicas consideradas quantificam separadamente alguns parâmetros de canal, tais como amplitudes complexas de desvanecimento, resposta do agregado de transmissão e receção. Depois disso, estes parâmetros quantizados são enviados para o transmissor e o canal é reconstruído para calcular o beamforming de transmissão. Os resultados mostraram que um número muito baixo de bits é necessário para obter um desempenho próximo ao obtido com informações de canal perfeito.

Keywords 5G, millimeter waves, massive MIMO, quantization

Abstract

The increase of electronic devices with wireless connections, end up presenting problems to the current architectures. The current 4G architecture can not handle the demands that arise from the increase of users and it will be necessary to deal with higher traffic and connections with higher transmission rate. Consequently, to meet these requirements, new technologies and techniques are needed for the next generation(5G).

Techniques such as the use of millimeter waves, combined with terminals equipped with large antenna arrays or massive number of antennas, although promising and presenting good results, bring with them new problems. Millimeter waves due to the smaller wavelength will allow systems with massive number of antennas. New transmit and receive signal processing (e.g. hybrid beamforming) has been proposed for millimeter wave communications combined with a massive number of antennas. However, transmit beamforming requires the knowledge of channel state information prior to the transmission. Therefore the design of efficient feedback techniques is of paramount importance for pratical systems. This issue is more relevant for massive MIMO based systems than for the conventional MIMO systems. For the first one the channel information to fed back is much higher.

In this dissertation a low-overhead feedback channel quantization scheme is proposed. Then, a single-user mmW massive MIMO system is evaluated under the developed quantization strategy. It was considered a transmitter employing a hybrid analog-digital equalizer. The considered techniques quantizes separately some channel parameters, such as complex fading amplitudes, transmit and receive array response. After that, these quantized parameters are fed back to the transmitter and the channel is reconstructed in order to compute the transmit beamformers. The results have shown that a very low number of bits is needed to obtain a performance close to the one obtained with perfect channel information.

Contents

List of Figures

List of Tables

List of Acronyms

1G 1st Generation

2D Two-Dimensional

2G 2nd Generation

3D Three-Dimensional

3G 3rd Generation

3GPP 3rd Generation Partnership Project

4G 4th Generation

5G 5th Generation

AA Antenna Array

ADC Analog-to-Digital Converter

AMPS Advanced Mobile Phone Service

AoA Angle of Arrival

AoD Angle of Departure

AWGN Additive White Gaussian Noise

BER Bit Error Rate

BS Base Station

CDI Channel Direction Information

CDMA Code Division Multiple Access

CFR Channel Frequency Response

CIR Channel Impulse Response

CoMP Coordinated Multipoint

CSI Channel State Information

CSIT Channel State Information at the Transmitter

DL Downlink

DoF Degrees of Freedom

DTF Discrete Fourier Transformation

EDGE Enhanced Data Rate for Global Evolution

eICIC enhanced Inter Cell Interference Coordination

EGC Equal Gain Combining

EGOS Equal Grade Of Service

EPS Evolved Packet System

EV-DO Evolution Data Optimized

FDD Frequency Division Duplex

FDMA Frequency Division Multiple Access

FFT Fast Fourier Transform

GMSK Gaussian Minimum Shift Keying

GPRS General Packet Radio Services

GSM Global System for Mobile communications

HSPA High Speed Packet Access

IDFT Inverse Discrete Fourier Transformation

IF Intermediate Frequency

IoT Internet of Things

IP Internet Protocol

ISI Intersymbol Interference

ITU International Telecommunication Union

IUI Inter-User Interference

LTE Long Term Evolution

MAC Media Access Control

MCS-L1 Mobile Communication System L1

MIMO Multiple Input Multiple Output

MISO Multiple-Input Single-Outputl

MMIC Monolithic Microwave Integrated Circuits

mmW millimeter Waves

MMSE Minimum Mean Square Error

MRC Maximal Ratio Combining

MSE Mean Square Error

NMT Nordic Mobile Telephony

NTT Nippon Telephone and Telegraph

OFDM Orthogonal Frequency Division Multiplexing

PSK Phase-Shift Keying

SMS Short Message Service

TDMA Time Division Multiple Access

PMI Precoding Matrix Indicator

PSK Phase-Shift Keying

QAM Quadrature Amplitude Modulation

QoS Quality of Service

QPSK Quadrature Phase-Shift Keying

RAN Radio Access Network

RAT Radio Access Technology

RF Radio Frequency

RVQ Random Vector Quantization

SAE System Architecture Evolution

SFBC Space Frequency Block Codes

SIMO Single-Input Multiple-Output

SISO Single-Input Single-Output

SNR Signal Noise Ratio

SQNR Signal-to-Quantization-Noise Ratio

STBC Space Time Block Codes

SVD Singular Value Decomposition

TDD Time Division Duplex

UL Uplink

ULA Uniform Linear Array

UMTS Universal Mobile Terrestrial System

UPA Uniform Planar Array

UQ Uniform Quantization

UT User Terminal

WCDMA Wideband Code-Division Multiple Access

WiMAX Worldwide Interoperability for Microwave Access

WLAN Wireless Local Area Networks

Chapter 1

Introduction

In this chapter, firstly it is showed the evolution of mobile communication systems, from how they started to how they lie now. Then, it is described two key technologies for the future cellular systems. In the end, the motivations, objectives, as well a brief summary of the following chapters are presented.

1.1 Evolution of Mobile Communication Systems

In 1857, Clark Maxwell inferred a hypothesis of electromagnetic radiation, which G. Marconi utilized as a premise for the creation of radio transmission in 1901, but was only in the late 1940's in the United States and in the 1950's in Europe, that the early "portable" telephones were presented [1]. Mobile and cellular communication systems, were a big change, and revolutionized the way people communicate. The cellular wireless generation (G) generally refers to a change in the fundamentals nature of the service, non-backwards compatible transmission technology, and new frequency bands. New generations have appeared in every ten years, since the first move from 1981, an analog (1G) to digital (2G) network. After that there was (3G) multimedia support, spread spectrum transmission and in 2011 all-IP switched networks (4G) came [2].

The first generation (1G) was completely analogous in nature. The first cellular system released in 1979 , was the NTT (Nippon Telephone and Telegraph) in Tokyo, Japan [2]. Two years later, in 1981, the first international mobile communication system was the analog NMT system (Nordic Mobile Telephony) which was introduced in the Nordic countries, at the same time as analog AMPS (Advanced Mobile Phone Service) was introduced in North America [3]. In Japan and Northen Europe, was introduced MCS-L1 (Mobile Communication System L1). These different systems, were similar and worked on the same rules, but only the NMT allow that the users from different operators, had proper function of their cell phones in other operator cover area, and outside theirs. With an international system such as NMT, came the concept of roaming, this gave a larger market for the mobile phones, attracting more companies into the mobile communication business [3].

In the early 1990's, as digital technology became more prevalent, analog 1G systems were replaced by the 2G digital systems. This new systems offered better voice quality [4] and the first data transmissions, that allowed short text messages to be send between users, this was

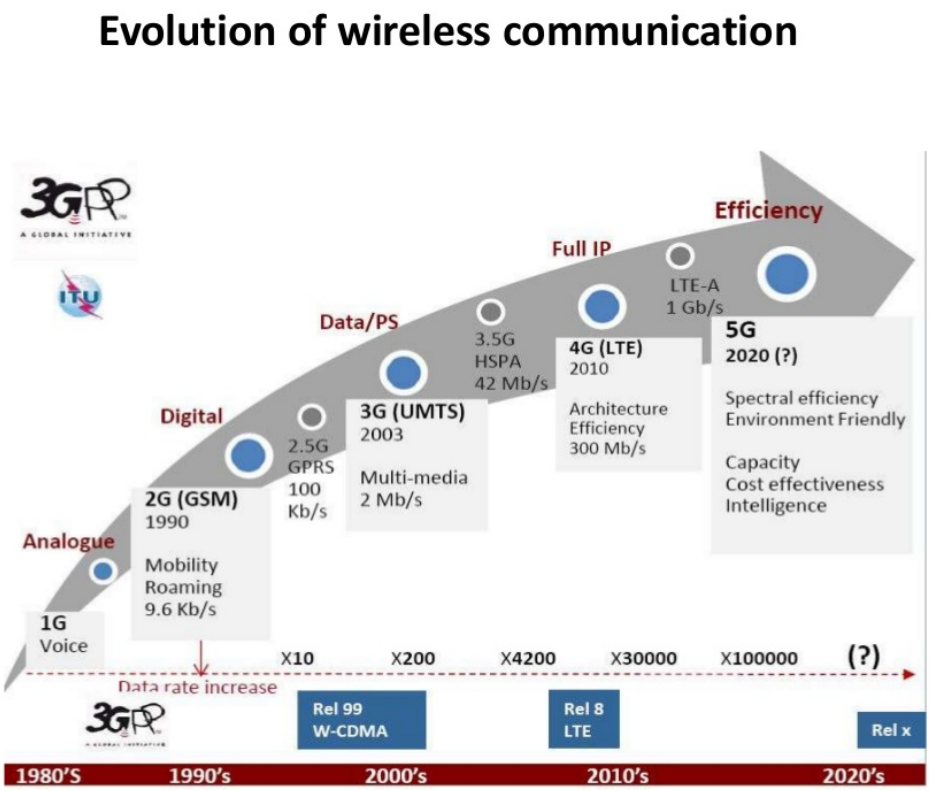

Figure 1.1: Evolution of wireless communication [5]

called Short Message Service (SMS). The 2G offered a better data service, higher spectrum efficiency and a more advanced roaming, so in Europe a working group (the Groupe Special Mobile) started the GSM project, to develop a pan-European mobile-telephony system [3]. The GSM became the most appreciated and used standard, it is utilized as a part of more than 212 nations [1]. The digital nature of 2G systems enabled the use of time and frequency division alternatives to separate users. After evaluations of TDMA, CDMA, and FDMA based proposals, the final GSM standard was built on TDMA. The peak data rates in 2G were initially 9.6 kbps [3], but later, during the second half of the 90's, packet data over cellular systems became a reality and General Packet Radio Services (GPRS) was intruduced in GSM. This became known as 2.5G and allowed data rates from 10 to 115 kbps. This was not enough, and the need for for higher data rates continue, this led to another evolution in 2G, called Enhanced Data Rate for Global Evolution (EDGE). EDGE can use GMSK or 8-ary PSK modulation, with each symbol representing three bits, this means that more data is transferred in each time slot [4].

In the EDGE, it was possible a high volume movement of data, but the air-interface make the packet transfer behaves like a circuit switches call, leading to low efficiency [2]. So in pursuit of higher data transfer and continuous evolution, 3G emerged. The 3G innova-

tion allowed better transmit packet switch information and expanded transmission capacity. Again, different standards were developed around different parts of the world. An organization called 3rd Generation Partnership Project (3GPP), grouped those standards to fulfill the IMT-2000 standard (unifying all wireless systems in the same frequency bands, including cellular, Wireless Local Area Networks (WLAN), satellite networks and fixed wireless links) [4]. The Universal Mobile Terrestrial System (UMTS) was the standard used in Europe. To get rates greater than 2 Mbps, UMTS incorporate Wideband Code-Division Multiple Access (WCDMA). In USA was used CDMA200, CDMA2 One Carrier Radio Transmission Technology (1xRTT). Later, both UMTS and 1xRTT evolved respectively to HSPA (High Speed Packet Access) and EV-DO (Evolution Data Optimized). This became known as 3.5G.

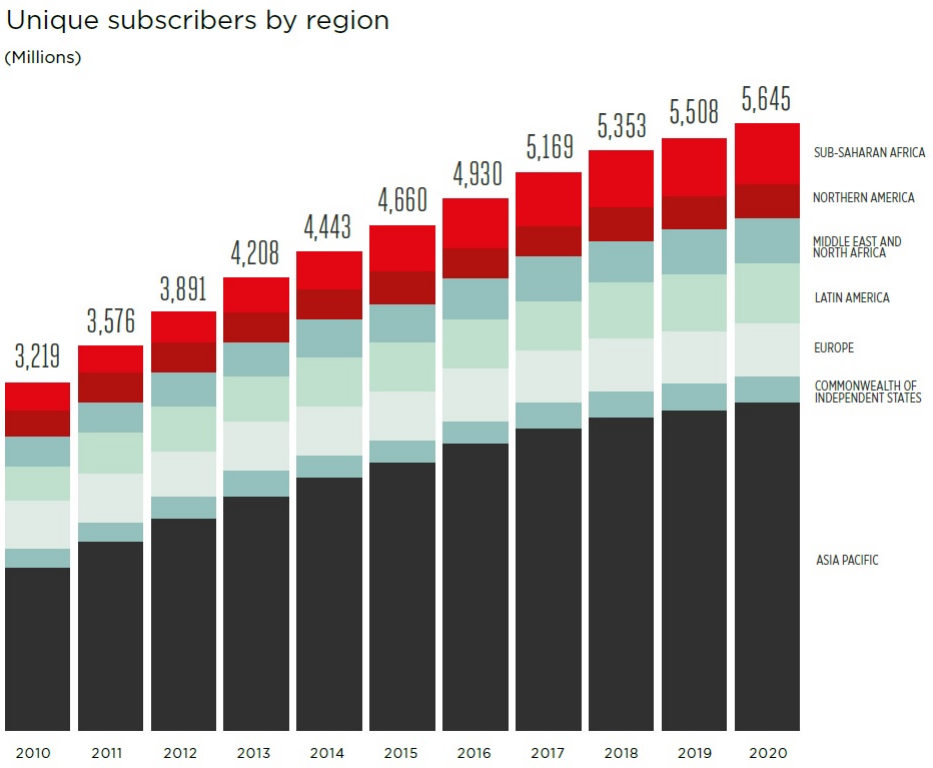

Figure 1.2: Evolucion of Subscribers by Region [6]

With the increasing demand for mobile broadband services with better quality and higher data rates, two new projects were started by 3GPP, the Long Term Evolution (LTE) and System Architecture Evolution (SAE). Known as Evolved Packet System (EPS), this new system include Orthogonal Frequency Division Multiplexing (OFDM) waveforms, so the intersymbol interference can be avoided. This represented a step forward to provide a highly efficient, packed-optimized, more secure and low-latency service. The first data services, like was mentioned before, were circuit switched or later packet-switched services. With HSPA and LTE, services over IP were made the priority design target [7]. LTE was required to deliver a peak data rate of 100 Mbps in the downlink and 50 Mbps in the uplink. This requirement was exceeded in this systems, which delivers peak data rates of 300 Mbps and

75 Mbps respectively [8].

In 2008, ITU (International Telecommunication Union) published a set of requirements for 4G under the name IMT-Advanced. These requirements stated that the peak data rate of a compatible system should be 600 Mbps on the downlink and 270 Mbps on the uplink [8] which exceeds the LTE capabilities. So, to pursuit those requirements, 3GPP started to study how to get that goal. With this study, came the system known as LTE-Advanced. LTE-Advanced was required to deliver a peak data rate of 1000 Mbps in the downlink, and 500 Mbps in the uplink. In 2010 ITU announced that two systems met the IMT-Advance requirements, the LTE-Advanced and the WiMAX 2.0, but LTE has greater support amongst network operators and is likely to be the world's dominant mobile communication technology for the next years [8].

1.2 Key technologies for future 5G systems

With this rapid increase of mobile data growth, the mobile users are creating challenges for wireless services providers. They are being asked to deliver high quality, low latency and multimedia applications for wireless devices, but they are limited between 700 MHz and 2.6 GHz in frequency spectrum [9]. This ever-growing consumer data rates demands, will need to be supported. Combining an efficient radio access technology and more spectrum available is the way to go. So to achieve this requirements with 5G, new disruptive technologies like millimeter waves (mmW) with the use of greater spectrum allocations and a new spatial processing techniques, such as massive MIMO (mMIMO) will be the key [10].

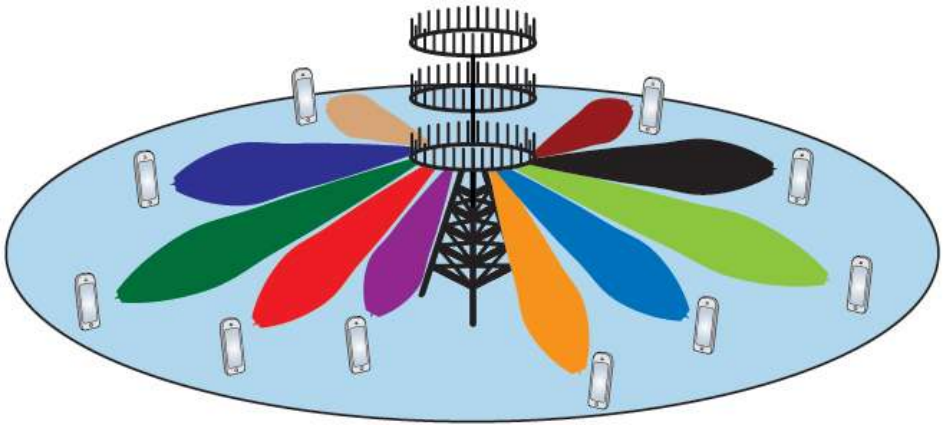

Figure 1.3: Massive MIMO system [11]

As the popularity of smart phones and other mobile data devices increases, the sub-3 GHz spectrum become increasingly crowded. On the other hand, the spectrum in the 3-300 GHz range remains underutilized [12]. For now this frequency range had not been used because of the propagation loss, like free-space or penetration loss, is higher in this interval. With shorter wave-lengths more antennas can be packed into the same area, so for the same antenna aperture areas, shorter wavelengths (higher frequencies) should not have

any inherent disadvantage compared to longer wavelengths (lower frequencies) in terms of free space loss [12]. The large antenna gain resulting from mMIMO can overcompensate the propagation difficulties of free space loss. The signal loss due to penetration, reflection and diffraction it is a mmWave problem. This kind of waves at high frequencies do not penetrate most solid materials like concrete or bricks, as a low frequency wave can. This may keep mmWaves confined to a outdoor scenario, and the indoor coverage can be made by femtocell or Wi-Fi solutions since his next generation will use 60 GHz mmWaves. In order to ensure a good coverage and reduces losses, the base stations in this mmWave system need to be in higher density than macrocells as we use now. Microcells or Picocells deployment are recommended. This cells, form a grid with more antennas to which an mobile can attach. It can be eliminated the problem of poor link quality at the cell edge and enables high-quality equal grade of service (EGOS) regardless the mobile location [12].

To achieve better gains massive MIMO systems have been deployed. Massive MIMO is a system where the number of antennas at the base station is much larger than the number of devices per signaling resource [10]. This number of antennas permit focusing energy into ever smaller regions of space to bring huge improvements in throughput. This kind of MIMO brings more benefits, like very simple spatial multiplexing/de-multiplexing procedures quasi-optimal, simplification of the MAC layer, use of inexpensive low-power components and reduced latency [10] [13].

1.3 Motivation and Objectives

With the rise of mobile devices, from smart phones to tablets, to the internet of things (IoT), there will be more and more wireless links. These links that will require higher speeds and larger amounts of data with better quality. Therefore, as mentioned above, millimeter waves and massive MIMO are two key technologies for future wireless systems in order to achieve these requirements. As already stated, the use of mmWs will allow large bandwidths and thus faster data transmissions. If we ally this kind of waves with a massive MIMO system, we can have beyond the faster data transmission, more advantages. It allows packing more antennas in the same volume due to the smaller wavelength compared to current microwave communication systems [10], and hence, the terminals can be equipped with large number of antennas. Moreover, the large antenna gain resulting from mMIMO can overcompensate the propagation difficulties of mmW communications.

MmW with massive MIMO may exploit new and efficient spatial processing techniques such as beamforming/precoding and spatial multiplexing at the transmitter and/or receiver sides. Hybrid analog/digital architectures, where some signal processing is done at the digital level and some left to the analog domain, have been considered for massive MIMO mmW systems. The use of hybrid analog-digital beamforming at transmitter side requires the knowledge of channel state information prior to transmission. This information can either be acquired by the base station (BS) in the uplink (UL) or by feedback of the user terminal (UT). The former is appropriate when considering time division duplex (TDD) due to the channel reciprocity in the UL and DL transmission periods and the latter for frequency division duplex (FDD) based systems. In either of these cases, it is important that the channel varia-

tions are sufficiently slow so that there are no considerable variations between the instant of acquisition and the usage of the channel. The knowledge of the CSI (Channel State Information) can then be used to improve the performance in the downlink. However, channel state information at the transmitter (CSIT) assuming a perfect CSIT, mainly for FDD systems, is not realistic in many practical scenarios. For the particular case of massive MIMO based systems this problem is more significant, since the terminal are equipped with a large number of antennas and therefore a huge amount of channels needed to be feedback from the receiver to the transmitter increasing the overall system signaling.

One possible solution to overcome this problem is feedback only a limited version of the antenna channels. Random vector quantization (RVQ) codebook [14] is a simple approach for the codebook design that generates the vectors independently from a uniform distribution on the complex unit sphere. Although RVQ techniques allow efficient precoding/beamforming schemes with limited feedback, the required codebooks can be very large, especially for a high number of transmit and receive antennas as for the case of massive MIMO systems. Although RVQ is often used in low frequency systems (sub-6GHz) is not the most efficient technique for massive MIMO systems. The uniform quantization-based (UQ) strategy for limited feedback, where the channels or just some channel parameters are quantized, it seems to be a better choice for these systems, since it has a good overhead/performance tradeoff comparatively to RVQ [15]. The aim of this dissertation is to evaluate a mmW massive MIMO link, where each terminal is equipped with a large number of antennas, under limited feedback. We consider a transmitter employing a hybrid analog-digital precoding/beamforming and a receiver equipped with a hybrid analog-digital equalizer, i.e. some processing is done at digital level and some is left for the analog part. One quantization strategy is implemented, which consists in the quantization of some channel parameters (e.g., amplitude, phases and delays). Then the system is evaluated under this CSI quantization strategy and compared with the case where perfect channel is known. This will give to us insights on how imperfect CSIT impacts on future hybrid mmW massive MIMO systems.

1.4 Outline of the dissertation

From this point forward, the dissertation stucture is organized in the following form:

In chapter 2, the MIMO systems are introduced, and some example schemes and main characteristics like diversity and multiplexing, followed by how it is used in LTE. The rest of the chapter will be reserved to basis about quantization, some of its principles, with reference to the particular cases of uniform quantization and random vector quantization.

Then in chapter 3, the features and advantages of millimeter waves and massive MIMO are explained in more detail. It is presented how they can be applied and how beneficial their combination can be. Finally, a mmWave channel model is presented.

Chapter 4, an hybrid massive MIMO mmWave platform, which was used to implement and evaluate the proposed channel quantization strategy. After that, it is explained the techniques used in this work, the quantization of individual channel parameters. To conclude

this chapter, the performance results of the technique is presented.

At the end, in chapter 5, the conclusions of this work and some guidelines for the future research are presented.

1.5 Notation

In this dissertation the following notation will be used: Italic lowercase letters, boldface lowercase letters and boldface uppercase letters are used for scalars, vectors and matrices, respectively. $(.)^T, (.)^H, (.)^*$ and $tr(.)$ represent the transpose, the Hermitian transpose, the conjugate and the trace of a matrix, $E[.]$ represents the expectation operator. Consider a matrix $\mathbf{A}$, diag($\mathbf{A}$) which correspond to a diagonal matrix with entries equal to the diagonal entries of matrix $\mathbf{A}$. $\mathbf{A}_{(n,l)}$ denotes the element at row n and column l of a matrix $\mathbf{A}$. $\mathbf{I}_N$ is the identity matrix of size $N \times N$.

Chapter 2

Multiple-antenna systems and Channel Quantization

Multiple antennas are an important means to improve the performance of wireless systems. It is widely understood that in a system with multiple transmit and receive antennas, the spectral efficiency is much higher than that of the conventional single antenna systems [16]. With this type of systems it is possible to explore spatial properties of the radio channels to improve the quality of service (QoS), and increase the data rates, to the mobile user. So in this chapter, it will be presented different types of multiple-antenna systems and how can those systems benefit from spatial properties, through diversity, spatial multiplexing and beamforming. Beamforming can improve the performance of the system, however the knowledge of channel state information at the transmitter is crucial, and assuming perfect CSIT is not realistic in many practical scenarios. Quantize the channel information and feedback it, can help to overcome the perfect CSIT problem.

2.1 Multi-Antenna Systems

Multiple-antenna systems can be used in four schemes, which differ between them according to the number of transmitter and receiver antennas. It can be seen in Figure 2.1, the four possible schemes, the Single-Input Single-Output (SISO), the Multiple-Input Single-Output (MISO), the Single-Input Multiple-Output (SIMO) and the Multiple-Input Multiple-Output (MIMO) scheme. With a higher number of transmitter and/or receiver antennas, the complexity rises, but each scheme has its advantages and disadvantages.

The SISO configuration is the simplest traditional form of radio link, but show more disadvantages in terms of fading and interference in comparison with the rest of the multiple-antenna schemes. Both the transmitter and the receiver are equipped with one antenna, so there is no much of spatial diversity, and the only one that can be used is repeating the symbols to send it in time or in frequency domains. One thing to keep in mind is that those copied symbols must be separated by a time/bandwidth separation, greater than the channel coherence time/bandwidth.

MISO is the scheme with multiple antennas on the transmitter side and one on the receiver. Is also known as the transmit diversity, because the same data is transmitted redundantly by

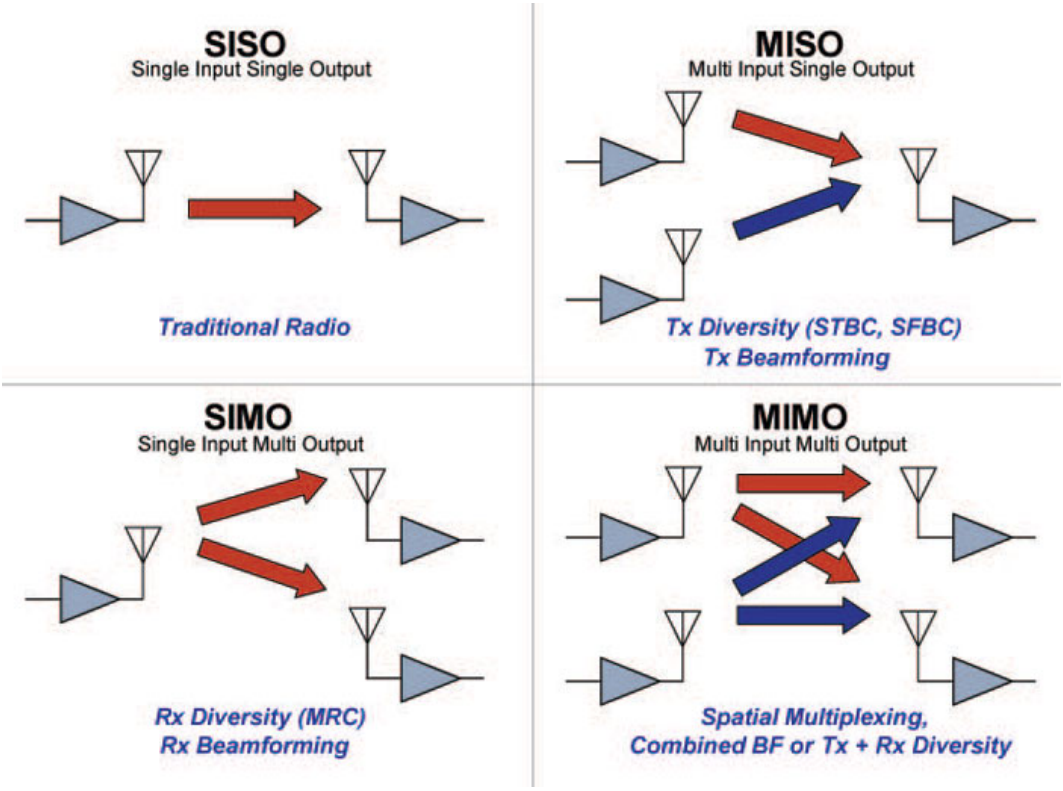

Figure 2.1: Multi-antenna schemes [17]

two or more antennas [18]. So this gives to the receiver the advantage to be able to reconstruct the original data from the signal that reach it in better conditions. MISO systems can exploit diversity when the CSI is known at the transmitter (beamforming), and when the CSI is not avaiable at the transmitter. In the case where CSI is not required at the transmitter, it can be used Space Time Block Codes (STBC) or Space Frequency Block Codes (SFBC) in order to achieve diversity gain, but no array gain. STBC/SFBC make use of blocks with coded symbols, with each symbol repeated in different time/frequency-space. The different symbols are transmitted through independent channels, which will create an interference problem [19]. To cancel the interference, some orthogonal codes are used, like the Alamouti code or the Tarokh code, which will be explained in another section.

In SIMO occurs the opposite of MISO, since all the complexity is on the receiver side. The SIMO configuration is known as receive diversity. In the same way as MISO, SIMO also decrease the influence of the multipath channel effect, and it can be used time and frequency diversity but also spatial diversity. Assuming that the receiver is able to acquire the perfect knowledge of the channel, two combining methods are used in order to exploit receive diversity. One of the methods is selection combining, which consists in select the branch with higher SNR (Signal Noise Ratio) among the received signals, and the other is equal gain combining, where the signal used is a linear combination of all branches [20].

When it is used more than one transmitting antenna and one receiving antenna, we are in

the case of a MIMO scheme. Multiple Input refers to the number of transmit antennas that transmit the radio signal and Multiple Output antennas to that send that signal. Although a superior number of antennas increases the complexity of the system, the high number of paths are now used advantageously. The paths can be used to provide additional robustness to the radio signal, improving the SNR or by increasing the capacity of the data connection. To get these improvements a good balance between diversity gain, multiplexing gain and beamforming is advisable.

2.2 Diversity

The technique of communications systems, known as diversity, consists in sending the same information for different channels in order to combat channel fading. By increasing the number of independent paths and sending signals that carry the same information through those multiple independent paths, different faded replicas can be obtained at the receiver, resulting in a more reliable reception. Both transmitter and receiver diversity, have the objective to combat fading and a system has a maximum diversity gain equal to the product between the number of transmit antennas M_t and the receiver antennas M_r [16].

By using multiple antennas at the transmitter, the amount of fading is reduced and the received signal power increases. There are three types of diversity that can be used. The temporal diversity is achieved when the same information its sent at different times, ensuring they are separated above the coherence time. In frequency diversity, the same signal is transmitted at different frequencies, and these frequencies must be spaced by more than the coherence bandwidth of the channel. The last one is spatial diversity, where the transmit signal is received at different antennas. In any process method, the performance is influenced by correlation of the signals between the antennas elements, so a large correlation between signals is undesirable. Spatial diversity, instead time diversity and frequency diversity, do not decrease the data rate or increase the bandwidth [21] [22].

2.2.1 Transmit Diversity

As it was said before, transmit diversity uses two or more antennas at the transmitter side, and the signal is transmitted to the receiver side. To achieve diversity there are two possible scenarios, with closed loop and with open loop.

With closed loop, two or more copies of the signal are sent by the transmitter, applying a phase shift to one or more signals before the transmission. This technique, can ensure that the risk of destructive interference is avoided because the signals are send in phase. For a closed-loop transmit diversity system, the receiver assists in channel estimation and feedback of these estimates to the transmitter. Thus, a reduced-complexity estimation and feedback process at the receiver along with simple processing at the transmitter will reduce consumption of system resources and result in an efficient communication system [23]. For LTE, the closed loop transmit diversity also occurs when the CSI is known at the transmitter, so to calculate the phase shift, the receiver through a precoding matrix indicator (PMI) calculate it and fed

back that information to the transmitter [8]. When the transmitter has the knowledge of the CSI, beamforming can be performed to achieve both diversity and array gains [20].

An open loop scenario, bring some advantages, that a closed one do not have, like not require the CSI knowledge, or robustness against adverse conditions. As discussed previously, to get transmit diversity there are some important techniques that can be used. For example with a system with two antennas at the transmitter it can be used the a STBC technique called Alamouti coding [24].

Alamouti coding aim to give orthogonal feature to data-stream, which bring symbol separation at the receiver.

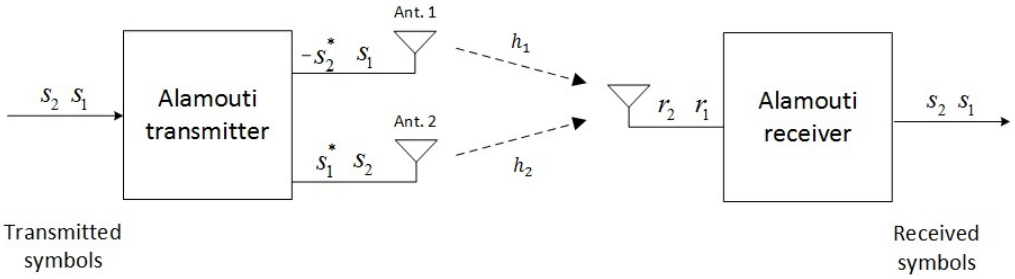

Figure 2.2: Alamouti scheme

As is shown in the Figure 2.2, the matrix that is sent by the transmitter is

$$\mathbf{S} = \begin{bmatrix} s_1 & -s_2^* \\ s_2 & s_1^* \end{bmatrix}, \tag{2.1}$$

From (2.1), at the first instant the symbols transmitted are s_1 and s_2 respectively by antenna 1 and 2, then at the second instant $-s_2^*$ and s_1^* are sent again by antenna 1 and 2. It can be find that those coded symbols are orthogonal

$$s_1 s_2 \; - \; s_1^* s_2^* \; = 0, \tag{2.2}$$

being h_1 the channel between the transmitter antenna 1 and the receiver antenna, and h_2 the channel for antenna 2, and n_1 and n_2 the noise for each antenna. The received signals before the Alamouti receiver is ($\frac{1}{\sqrt{2}}$ is the power constraint to normalize the power per symbol to 1)

$$\begin{cases} r_1 = \frac{1}{\sqrt{2}} h_1 s_1 + \frac{1}{\sqrt{2}} h_2 s_2 + n_1 \\ r_2 = \frac{1}{\sqrt{2}} - h_1 s_2^* + \frac{1}{\sqrt{2}} h_2 s_1^* + n_2 \end{cases}, \tag{2.3}$$

After the Alamouti decoder is given by

$$\begin{cases} \hat{s}_1 = \frac{1}{\sqrt{2}} h_1^* r_1 + \frac{1}{\sqrt{2}} h_2 r_2^* \\ \hat{s}_2 = \frac{1}{\sqrt{2}} h_2^* r_1 - \frac{1}{\sqrt{2}} h_1 r_2^* \end{cases}, \tag{2.4}$$

consequently, the soft decision of data symbol is

$$\hat{s}_n = \frac{1}{2}(h_1^* h_1 + h_2 h_2^*)s_n + \frac{1}{\sqrt{2}}h_1^* n_1 + \frac{1}{\sqrt{2}}h_2 n_2^*, \tag{2.5}$$

with this the interference created by the data symbol n+1 is full eliminated, and the SNR is given by

$$SNR = \frac{1}{2}\frac{(|h_1|^2 + |h_2|^2)}{\sigma^2}, \tag{2.6}$$

Alamouti codes can be only used for the case where the transmitter is equipped with 2 antennas. For more than 2 antennas, Tarokh orthogonal codes or Quasi-Orthogonal codes can be used [25] [26]. Tarokh codes although being orthogonal such as Alamouti codes, and can be used for more than two transmitter antennas, have the disadvantage of having a code rate less than 1, therefore it is required a bandwidth expansion. To overcome this code rate and required bandwidth expansion problem, some Quasi-orthogonal codes were proposed, where the code rate is 1, but they can't obtain full diversity. The code ratio is defined as the ratio between the number of symbols the encoder takes as its input, N_s, and the number of symbols transmitted from each antenna N_p

$$R = \frac{N_s}{N_p}, \tag{2.7}$$

Tarohk codes, which are an orthogonal code with code rates lower than 1, bring advantages but also some costs. Having a code rate lower than 1 bring advantages such as achieve full orthogonality between the streams in each antenna, making full diversity order possible, but at cost of a bandwidth increase or transmission rate decrease [19].

For example, a system with 4 transmit antennas and 1 receiver the code rate is $R = 1/2$, the Tarohk coding matrix is

$$\mathbf{S} = \begin{bmatrix} s_1 & -s_2 & -s_3 & -s_4 & s_1^* & -s_2^* & -s_3^* & -s_4^* \\ s_2 & s_1 & s_4 & -s_3 & s_2^* & s_1^* & s_4^* & -s_3^* \\ s_3 & -s_4 & s_1 & s_2 & s_3^* & -s_4^* & s_1^* & s_2^* \\ s_4 & s_3 & -s_2 & s_1 & s_4^* & s_3^* & -s_2^* & s_1^* \end{bmatrix}, \tag{2.8}$$

Then the received signals are

$$\begin{cases} y_1 = h_1 s_1 + h_2 s_2 + h_3 s_3 + h_4 s_4 + n_1 \\ y_2 = -h_1 s_2 + h_2 s_1 - h_3 s_4 + h_4 s_3 + n_2 \\ y_3 = -h_1 s_3 + h_2 s_4 + h_3 s_1 - h_4 s_2 + n_3 \\ y_4 = -h_1 s_4 - h_2 s_3 + h_3 s_2 + h_4 s_1 + n_4 \\ y_5 = h_1 s_1^* + h_2 s_2^* + h_3 s_3^* + h_4 s_4^* + n_5 \\ y_6 = -h_1 s_2^* + h_2 s_1^* - h_3 s_4^* + h_4 s_3^* + n_6 \\ y_7 = -h_1 s_3^* + h_2 s_4^* + h_3 s_1^* - h_4 s_2^* + n_7 \\ y_8 = -h_1 s_4^* - h_2 s_3^* + h_3 s_2^* + h_4 s_1^* + n_8 \end{cases}, \tag{2.9}$$

And the soft decision can be obtained from

$$\begin{cases} \hat{s_1} = y_1 h_1^* + y_2 h_2^* + y_3 h_3^* + y_4 h_4^* + y_5^* h_1 + y_6^* h_2 + y_7^* h_3 + y_8^* h_4 \\ \hat{s_2} = y_1 h_2^* - y_2 h_1^* - y_3 h_4^* + y_4 h_3^* + y_5^* h_2 - y_6^* h_1 - y_7^* h_4 + y_8^* h_3 \\ \hat{s_3} = y_1 h_3^* + y_2 h_4^* - y_3 h_1^* - y_4 h_2^* + y_5^* h_3 + y_6^* h_4 - y_7^* h_1 - y_8^* h_2 \\ \hat{s_4} = -y_1 h_4^* - y_2 h_3^* + y_3 h_2^* - y_4 h_1^* - y_5^* h_4 - y_6^* h_3 + y_7^* h_2 - y_8^* h_1 \end{cases}, \tag{2.10}$$

As it was said, the diversity of 4 can be achieved but the bandwidth was doubled. If the code used is not orthogonal, at the decoder, all transmitted symbols cannot be separated from each other. Instead if a quasi-orthogonal code is used, the transmission matrix columns are divided into groups. The elements of these groups are not orthogonal with each other, but the different groups are orthogonal to each other.

In Quasi-Orthogonal code proposed in [27], for example if there are 4 antennas at the transmitter and 1 at the receiver the coding matrix is

$$\mathbf{S} = \begin{bmatrix} s_1 & s_2 & s_3 & s_4 \\ s_2^* & -s_1^* & s_4^* & -s_3^* \\ s_3 & s_4 & s_1 & s_2 \\ s_4^* & -s_3^* & s_2^* & -s_1^* \end{bmatrix}, \tag{2.11}$$

and the received signals are

$$\begin{cases} y_1 = h_1 s_1 + h_2 s_2 + h_3 s_3 + h_4 s_4 + n_1 \\ y_2 = h_1 s_2^* - h_2 s_1^* + h_3 s_4^* - h_4 s_3^* + n_2 \\ y_3 = h_1 s_3 + h_2 s_4 + h_3 s_1 + h_4 s_2 + n_3 \\ y_4 = h_1 s_4^* - h_2 s_3^* + h_3 s_2^* - h_4 s_1^* + n_4 \end{cases}, \tag{2.12}$$

In matrix notation

$$\begin{bmatrix} y_1 \\ y_2^* \\ y_3 \\ y_4^* \end{bmatrix} = \begin{bmatrix} h_1 & h_2 & h_3 & h_4 \\ -h_2^* & h_1^* & -h_4^* & h_3^* \\ h_3 & h_4 & h_1 & h_2 \\ -h_4^* & h_3^* & -h_2^* & h_1^* \end{bmatrix} \times \begin{bmatrix} s_1 \\ s_2 \\ s_3 \\ s_4 \end{bmatrix} + \begin{bmatrix} n_1 \\ n_2 \\ n_3 \\ n_4 \end{bmatrix}, \tag{2.13}$$

So the received signal is,

$$\mathbf{y} = \mathbf{H}_{eq} s + \mathbf{n}, \tag{2.14}$$

where

$$\mathbf{H}_{eq}^H \mathbf{H}_{eq} = h_{eq} \begin{bmatrix} 1 & 0 & X & 0 \\ 0 & 1 & 0 & X \\ X & 0 & 1 & 0 \\ 0 & X & 0 & 1 \end{bmatrix}, \tag{2.15}$$

and

$$h_{eq} = h_1^2 + h_2^2 + h_3^2 + h_4^2, \tag{2.16}$$

$$X = \frac{2Re(h_1 h_3^* + h_2 h_4^*)}{h_{eq}^2}, \tag{2.17}$$

The use of quasi-orthogonal codes, provide higher transmission rates, while sacrifice full diversity.

2.2.2 Receive Diversity

The use of M_r antennas at the receiver allow the reception of symbols across M_r channels, this bring spatial diversity at the reception. This type of diversity allows to decrease the influence of the multipath channel effect [19]. As it can be seen if Figure 2.3 the received signal model is,

$$\begin{bmatrix} y_1 \\ \vdots \\ y_{M_r} \end{bmatrix} = \begin{bmatrix} h_1 \\ \vdots \\ h_{M_r} \end{bmatrix} s + \begin{bmatrix} n_1 \\ \vdots \\ n_{M_r} \end{bmatrix}, \tag{2.18}$$

with the estimated symbols being,

$$\hat{s} = [g_1 \ ... \ g_{M_r}] \begin{bmatrix} y_1 \\ \vdots \\ y_{M_r} \end{bmatrix}, \tag{2.19}$$

$$\hat{s} = [g_1 \ ... \ g_{M_r}] \begin{bmatrix} y_1 \\ \vdots \\ y_{M_r} \end{bmatrix} + [g_1 \ ... \ g_{M_r}] \begin{bmatrix} n_1 \\ \vdots \\ n_{M_r} \end{bmatrix}, \tag{2.20}$$

To combine the multiple received signals there are some methods. The methods that show good results are the Equal Gain Combining (EGC) and the Maximal Ratio Combining (MRC).

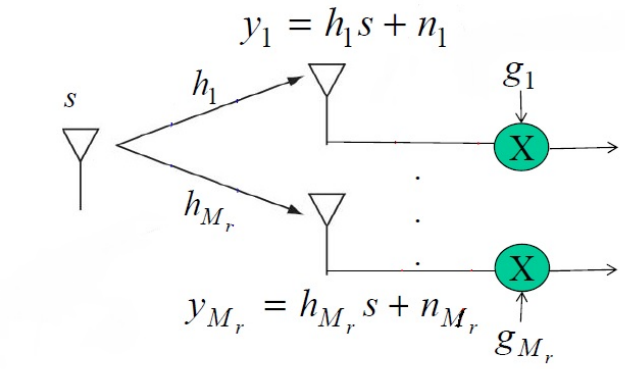

Figure 2.3: Receive Diversity [28]

2.2.3 Maximal Ratio Combining

MRC is a linear combining technique that compensates for the phases, and weights the signals from the different antenna branches according to their SNR in order to maximize it and eliminate bad noise conditions. In the uplink, MRC is the most promising single-user detection technique since the spreading codes do not superpose in an orthogonal fashion at the receiver and maximization of the signal-to-interference ratio is optimized [21] [22].

Using the model given by Figure 2.3, the received signals are,

$$y_1 = \mathbf{h}_1 s + n_1, \tag{2.21}$$

$$\vdots$$

$$y_{M_r} = \mathbf{h}_{M_r} s + n_{M_r}, \tag{2.22}$$

The optimal weights for maximal-ratio combining in fading is

$$g_m = h_m^* \qquad m = 1, ..., M_r, \tag{2.23}$$

and the diversity achievable with MRC at the output combiner is,

$$\hat{s} = \sum_{m=1}^{M_r} |h_m|^2 s + \sum_{m=1}^{M_r} h_m^* n_m, \tag{2.24}$$

The antenna gain will be equal to the number of M_r receiver channels.

2.2.4 Equal Gain Combining

This combining method co-phases the received signals at each antenna and combines them with equal weights, given by

$$g_m \frac{h^*}{|h|}, \qquad m = 1, ..., M_r, \tag{2.25}$$

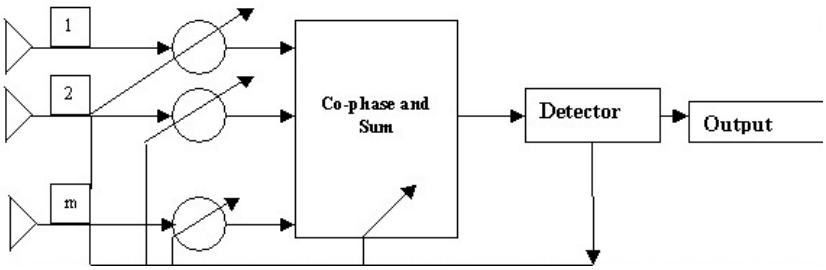

Figure 2.4: Receive Diversity - EGC [29]

At the output combiner, the signal is,

$$\hat{s} = \sum_{m=1}^{M_r} |h_m| s + \sum_{m=1}^{M_r} \frac{h_m^*}{|h_m|} n_m, \tag{2.26}$$

In this case the antenna gain is,

$$A_g = (1 + \frac{\pi}{4}(M_r - 1)), \tag{2.27}$$

ECG has a reduced complexity compared to MRC. Although they achieve the same diversity, it was proved that it has lower antenna gains. MRC has a slight better performance than the ECG.

2.3 Multiplexing

By transmitting independent information streams in parallel through the spatial channels, the data rate can be increased. This effect is called spatial multiplexing [16]. If the dispersion medium is high, the spatial multiplexing creates multiple subchannels within the same wide band defined at the outset. This creation of subchannels, known as multiplexing gain(or degree-of-freedom) does not lead to increased bandwidth, power or costs. In a $M_r \times M_t$ MIMO system where the channel is known at the transmitter, that channel consist of an $M_r \times M_t$ matrix given as:

$$\mathbf{H} = \begin{bmatrix} h_{11} & h_{12} & ... & h_{1M_t} \\ h_{21} & h_{22} & ... & h_{2M_t} \\ \vdots & \vdots & ... & \vdots \\ h_{M_r1} & h_{M_r2} & ... & h_{M_rM_t} \end{bmatrix}, \tag{2.28}$$

where h_{nl} represents the channel gain from trasmission antenna l to the receiver antenna n [30]. So the received signal is given by:

$$\mathbf{y} = \mathbf{H}\mathbf{x} + \mathbf{n}, \tag{2.29}$$

where $\mathbf{y} = [y_1, ..., y_{M_r}]^T$ is the signal received, $\mathbf{H}$ is the channel, $\mathbf{x} = [x_1, ..., x_{M_t}]^T$ is the transmitted signal, and $\mathbf{n} = [n_1, ..., n_{M_t}]^T$ is noise.

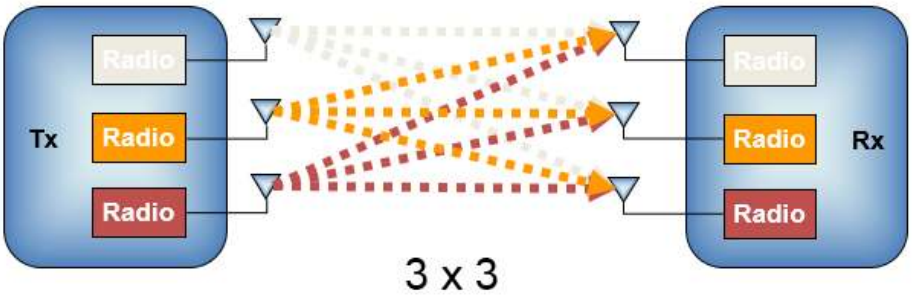

Figure 2.5: Spatial Multiplexing in a 3x3 MIMO System [31]

The channel can also be converted into a set of parallel channels. Using Singular Value Decomposition(SVD), the $\mathbf{H}$ matrix can be decomposed as,

$$\mathbf{H} = \mathbf{U}\mathbf{D}\mathbf{V}^T, \tag{2.30}$$

where $\mathbf{U}$ and $\mathbf{V}$ are unitary matrices of size $M_r \times r$ and $M_t \times r$,$\mathbf{D}$ is a diagonal matrix with non negative real numbers, and $r = rank(\mathbf{H}) \leq min(M_r, M_t)$. The transmitted signal x is defined as,

$$\mathbf{x} = \mathbf{W}\mathbf{s}, \tag{2.31}$$

where s is the data stream transmitted over the M transmit antennas($s = [s_1 \ ... \ s_r]^T$), and the precoder matrix $\mathbf{W}$ is,

$$\mathbf{W} = \mathbf{V}\mathbf{P}^{\frac{1}{2}}, \tag{2.32}$$

with size $M_t \times r$ and $\mathbf{P}$, a square diagonal power allocation matrix of size $r \times r$, is given by,

$$\mathbf{P} = \begin{bmatrix} p_1 & 0 & 0 \\ 0 & \ddots & 0 \\ 0 & 0 & p_r \end{bmatrix}^{\frac{1}{2}}, \tag{2.33}$$

At the receiver side the equalizer matrix can be computed as

$$\mathbf{G} = \mathbf{U}^H, \tag{2.34}$$

Using (2.30), (2.31) and (2.32), the received signal can be written as,

$$\mathbf{y} = \mathbf{U}\mathbf{D}\mathbf{V}^T\mathbf{V}\mathbf{P}^{\frac{1}{2}}\mathbf{s} + \mathbf{n}, \tag{2.35}$$

Then the estimated transmitted data symbols is obtained by,

$$\hat{\mathbf{s}} = \mathbf{G}\mathbf{y} = \mathbf{U}^T\mathbf{U}\mathbf{D}\mathbf{V}^T\mathbf{V}\mathbf{P}^{\frac{1}{2}}\mathbf{s} + \mathbf{U}^T\mathbf{n}, \tag{2.36}$$

$$\hat{\mathbf{s}} = \mathbf{D}\mathbf{P}^{\frac{1}{2}}\mathbf{s} + \tilde{\mathbf{n}}, \tag{2.37}$$

If the channel is known at the transmitter it can be seen that converting the channel into r parallel channels with SVD, it is possible to transmit r parallel free interference data symbols.

$$\hat{s}_i = \lambda_i\sqrt{p_i}s_i + \tilde{n}_i, \quad i = 1, ..., r, \tag{2.38}$$

It is not necessary to chose between antenna diversity or purely multiplexing, both can be used at the same time, but it is impossible to use them at full potential. If full diversity is used it means each symbol go through all independent channels, and there is no channels free to pass different symbols, multiplexing cant be done. The other way around the same thing happens, with full multiplexing each channel is used by different symbols and there is no channels left over to reach diversity. In the diversity, the data rate is constant and the BER decreases as the SNR increases and, in multiplexing, BER is constant while the data rate increases with SNR [32].

2.4 Beamforming

In order to increase cell coverage, a multiple antenna technique called beamforming can be used assuming that the CSI is available at transmitter. Beamforming is a powerful technique which increases the link signal-to-noise ratio through focusing the energy into desired directions [20]. This process is used by a array of sensors to provide spatial filtering. Spacial filtering is important to attenuate wireless interference, imagine when several rocks are thrown into a lake, the different circular waves that rocks create, will interfere with each other, and this is what is happening now with so many wireless devices. Too many interference's can create a unstable connection.

Based on MIMO technology and digital signal processing, beamforming can determine the better direction of the receiver device. To do this, the phase and amplitude of the signal is changed by a beamformer, usually the transmitter. Two types of interference are created with this changes, a construtive one and a destrutive, in order to make the signal stronger in the desired direction and weaker in the others, as it can be seen in Figure 2.8. MIMO

technology is a very important point in beamforming. Thanks to the number of antennas at the transmitter, different signals can be sent through these, to create a stronger one.

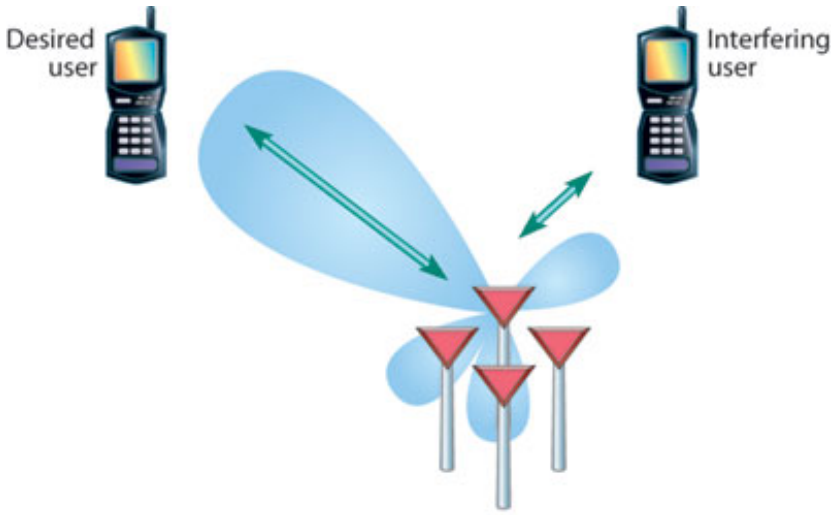

Figure 2.6: Beamforming Technique [33]

2.5 Signal Quantization Principles

Two types of quantization can be identified: uniform or non-uniform. In both cases the quantized signal, x_Q, can be defined as the sum of the signal intended to be quantized, x, with an interference error, ε_Q

$$x_Q = x + \varepsilon_Q, \tag{2.39}$$

Assuming uniform quantization, L levels are separated by a uniform step Δ. If the original signal, that we want to quantize, has a power of P_x and a mean value equal to zero, taking continuous values between $-A_M$ and A_M, where A_M is the maximum level of the original signal, then the step is $\Delta = 2A_M/L$. The signal is equally spaced in L intervals, $[a_i, a_{i+1}[, i = 1, ..., L$, with $a_i = A_M(\frac{2i-2}{2^b} - 1), i = 1, ..., 2^b$, where b is the number of quantization bits. The values of the signal x in each of the previous intervals are quantized to the following levels,

$$q_i = a_i + \frac{(a_i + 1 - a_i)}{2} = A_M(\frac{2i-1}{2^b} - 1), i = 1, ..., 2^b, \tag{2.40}$$

Thus the quantization characteristic function is given by

$$g(x) = \begin{cases} A_M & , if\ x \geq A_M \\ A_M(\frac{2i-2}{2^b} - 1) & , if\ x \in [a_i, a_{i+1}[, i \in 1, ..., 2^b \\ -A_M & , if\ x < -A_M \end{cases}, \tag{2.41}$$

Considering the quantized channel as $y = g(x) = \alpha x + d$, the average power of the useful signal is

$$S = |\alpha|^2 \sigma_x^2, \tag{2.42}$$

the average power of the quantized signal is

$$P_{out} = E[|y|^2] = \frac{1}{\sqrt{2\pi}\sigma} \int_{-\infty}^{+\infty} g^2(x) e^{-\frac{x^2}{2\sigma_x^2}} dx, \tag{2.43}$$

and the average power of quantization error is

$$P_s = P_{out} - S, \tag{2.44}$$

The factor α is given by

$$\alpha = \frac{E[y^* x]}{E[|x|^2]} = \frac{1}{\sqrt{2\pi}\sigma} \int_{-\infty}^{+\infty} x g(x) e^{-\frac{x^2}{2\sigma_x^2}} dx, \tag{2.45}$$

The generic characteristic is represented in Figure 2.7. For the uniform quantization the variance is given by $\sigma_\varepsilon^2 = \frac{\Delta^2}{12}$, where Δ is the amplitude of each quantization level.

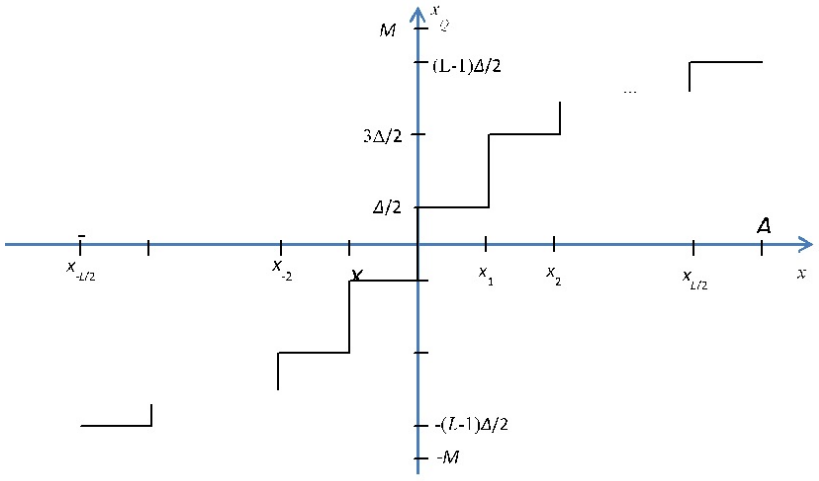

Figure 2.7: Characteristic function for uniform quantization

The characteristic quantization function can be represented as the one in Figure 2.8, when A_M is equal to 1.

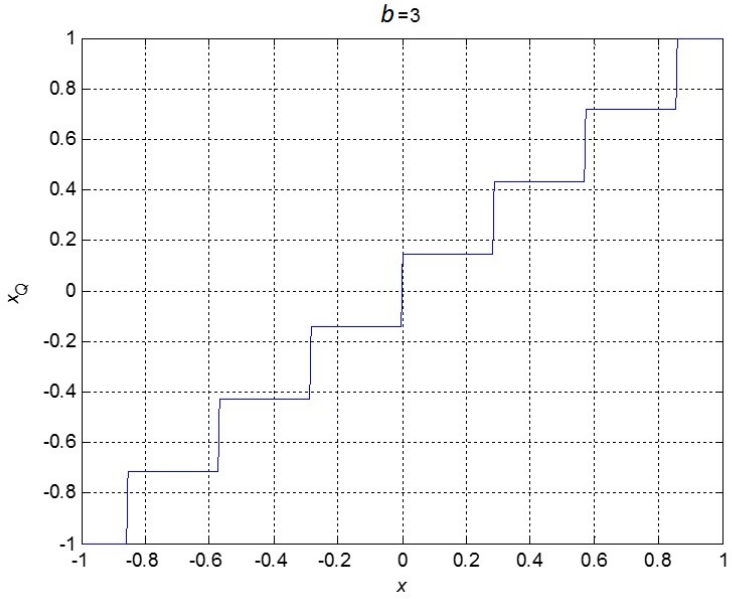

Figure 2.8: Characteristic function for uniform quantization for a saturation level of $A_M = 1$

The signal-to-quantization-noise ratio (SQNR) is given by

$$SQNR = \frac{P_x}{E[|x - x_Q|^2]} \tag{2.46}$$

and it is dependent on the saturation level, as we can observe in Figure 2.9

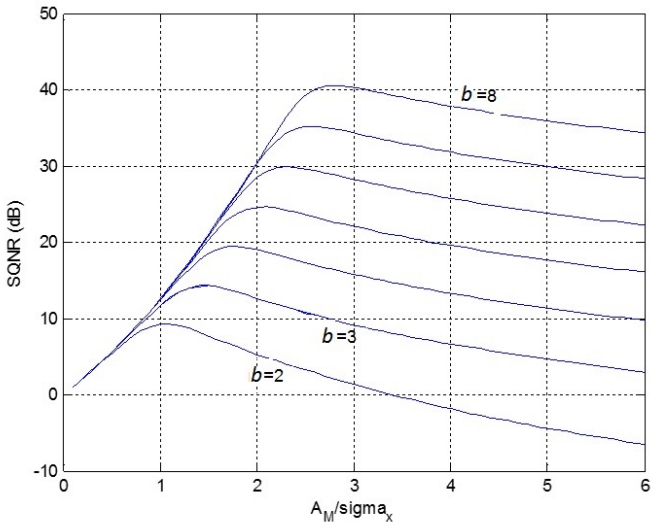

Figure 2.9: SQNR curve in function of normalized saturation level for uniform quantization of real signal

2.6 Channel Quantization

As discussed above, multi-antenna techniques are used to achieve diversity and/or multiplexing gains [22], [34]. Linear precoding is a generalization of beamforming at the transmitter used in this systems aiming to cancel interference between users or separate the data symbols [35]. However, the knowledge of channel state information at the transmitter is absolutely crucial for such techniques, and assuming perfect CSIT is not realistic in many practical scenarios. To overcome this drawback, recent studies addressed the issue of limited feedback in CSI exchange.

Limited feedback is a technique where the CSI is quantized and fed back to the transmitter through a limited link and was first introduced in [36]. To limit the overhead needed to feed back CSI it was considered that receiver and transmitter maintain a common codebook with a finite set of precoding matrices. The receiver chooses the optimal precoder from the codebook as a function of the current channel state information available at the receiver and sends the index of this matrix to the transmitter over a limited bandwidth control channel [37]. Random vector quantization is a simple approach of codebook design, firstly defined in [38], where the vectors are generated independently from a uniform distribution on the complex unit sphere [39]. The beamforming expressions for RVQ limited feedback in terms of average bit error probability and ergodic capacity for a MISO based system are derived in [39]. Although RVQ technique allows efficient limited feedback for multi-antenna, multi-user schemes, the required codebooks can be very large, especially when we have a high number of transmit and receive antennas. Another major drawback of RVQ is the required computational complexity. In that case, it is preferable to employ simpler uniform quantization methods, working on a sample-by-sample basis, as in [40].

2.6.1 System Model

An example of a multi-user MISO system with limited feedback is presented in this section. It is considered a single BS equipped with M_t antennas transmitting to K single antenna UTs sharing the same resources, as shown in Figure 2.10, with $M_t > K$.

The channel associated to the link between the BS and the kth UT is represented by the vector $\mathbf{h}_k \in \mathbb{C}^{M_t \times 1}$, with $k = 1, ..., K$. The quantized version of the channel is fed back using one of the quantization strategies described in the next section. Since the users share the same resources a precoding/beamforming technique should be employed at the transmitter in order to format the transmit signal in such a way that inter-user interference is cancelled or mitigated. Under linear precoding, the received signals for the overall UTs are given by

$$\mathbf{y} = \mathbf{HWs} + \mathbf{n}, \tag{2.47}$$

where $\mathbf{H} = [\mathbf{h}_1 \, \mathbf{h}_2 \, ... \, \mathbf{h}_K]^T$, with $\mathbf{H} \in \mathbb{C}^{K \times M_t}$, is the equivalent channel that contains the flat Rayleigh fading coefficients with i.i.d. $\mathcal{CN}(0,1)$ entries; $\mathbf{s}$ is the data symbols vector, with $\mathbf{s} \in \mathbb{C}^{K \times 1}$ and $E[\mathbf{s} \, \mathbf{s}^H] = \mathbf{I}_K$; $\mathbf{W} \in \mathbb{C}^{M_t \times K}$ is the linear Minimum Mean Square Error

(MMSE) precoding matrix computed at the BS calculated by

$$\mathbf{W} = \alpha(\mathbf{H}^Q)^H(\mathbf{H}^Q(\mathbf{H}^Q)^H + \sigma^2\mathbf{I}_K)^{-1}, \tag{2.48}$$

where $\mathbf{H}^Q$ is the equivalent channel after quantization; $\mathbf{n}$ is the additive white Gaussian noise (AWGN) vector and α is a normalization factor such that $\mathrm{tr}(\mathbf{W}^H\mathbf{W}) = 1$. The overall channel matrix, when taking into account the channel quantization errors, can be modeled as $\mathbf{H}^Q = \mathbf{H} + \mathbf{E}^Q$ where $\mathbf{E}^Q$ is the overall quantized error matrix.

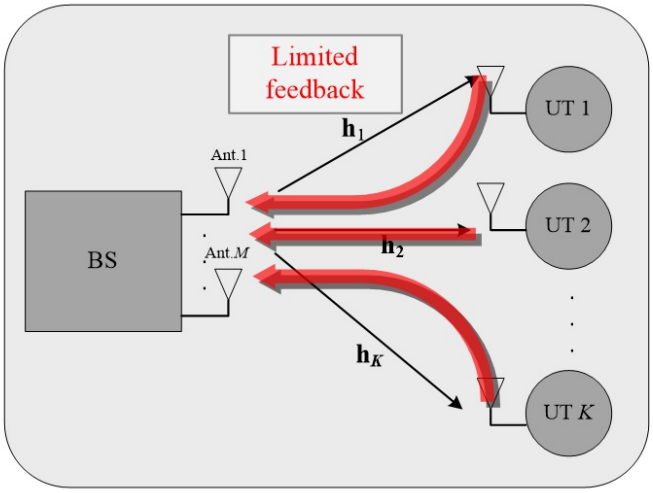

Figure 2.10: Multi-user MISO system model

2.6.2 Random Vector Quantization

As mentioned RVQ is a simple approach of codebook design that generates the vectors independently from a uniform distribution on the complex unit sphere. Although RVQ techniques allow efficient multi-antenna multi-user schemes with limited feedback, the required codebooks can be very large, especially when we have a high number of transmit and receive antennas. Another major drawback of RVQ is its computational complexity.

In this section we briefly describe the RVQ feedback quantization technique often considered for MIMO based systems. The constructed codebook for channel direction information (CDI), defined as the normalized CSI (i.e. $\mathbf{h}_k^d = \mathbf{h}_k/|\mathbf{h}_k|$), is formed by 2^b vectors i.i.d. on the M-dimensional unit sphere, $\mathbf{c}_b, b = 1, ..., 2^b$, where b represents the number of feedback bits per user. Each user quantizes its CDI to a codeword in a given codebook $\mathbf{C}_k \in \mathbb{C}^{M_t \times 2^b}$ and the codebook is predetermined and known at both the BS and user sides. Partial CSI is acquired at the transmitter via a finite rate feedback channel from each of the receivers. Furthermore we use the minimum Euclidean distance to choose the codeword closest to each

channel vector direction, i.e.,

$$f = arg \min_{i=1,...,2^b} ||\mathbf{h}_k^d - \mathbf{c}_i||^2, \tag{2.49}$$

with $k = 1, ..., K$. Thus, after each UT having sent the index of the codeword to the BS, the BS obtain the CSI through the corresponding codebooks and using the indexes given by $\mathbf{h}_k^Q = \mathbf{c}_{f_k}$, so that it can design the precoder matrices. Only the CDI is sent, dismissing the channel magnitude information with this method.

2.6.3 Uniform Quantization

Considering severely time-dispersive channels or terminals equipped with a large number of antennas RVQ is not the most efficient method to quantize the channels. For this type of scenario UQ is preferable, where only some parts of the channel frequency response (CFR) and/or channel impulse response (CIR) are quantized. For example assuming OFDM systems with N_c carriers, RVQ requires the quantization of the N_c samples for each antenna link. It is well known that the channel CIR has a duration that must be smaller than the duration of the cyclic prefix, N_{CP}, which for typical OFDM implementations is much lower than N_c. Therefore, CIR must be zero for taps higher than N_{CP}. Therefore, when $N_c > N_{CP}$ it is enough to sample the CFR at a rate N_c/N_{CP}, i.e., is only needed $N_s = N_{CP}$ equally spaced samples of the CFR to obtain it without loss of information [40] [15]. Thus, this method only quantizes equally spaced samples of the CFR (i.e., quantize the CFR samples on positions $(0, N_c/N_{CP}, 2N_c/N_{CP}, ...)$. From the samples chosen to be quantized $h_{k,l\Delta f_s}; l = 0, 1, ..., N_s - 1$, with $\Delta f_s = N_c/N_s$, is obtained $h_{k,l}^Q; l = 0, 1, ..., N_s - 1$ considering the separate quantization of the real and imaginary parts of each of the appropriate samples as following

$$h_{k,l}^Q = f_Q(Re\{h_{k,l\Delta f_s}\}) + j f_Q(Im\{h_{k,l\Delta f_s}\}), \tag{2.50}$$

where $f_Q(.)$ denotes the quantization characteristic.

If we consider the use of b quantization bits for each real and imaginary parts of each sample for the UQ technique and B bits for each user for RVQ, the total number of bits required for CSI quantization with UQ is $2bKM_tN_s$ and with RVQ is bKN_c bits.

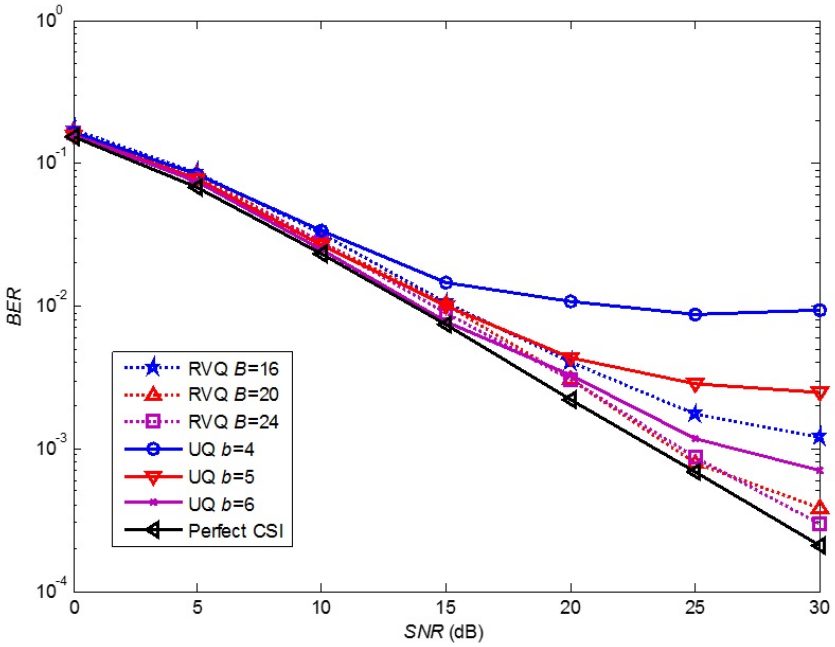

Figure 2.11: BER performances using RVQ and UQ for $M_t = 2$ and K=2 [40]

Figure 2.11 presents the BER performance of these two approaches, for the precoding multi-user MISO system, when using the same amount of quantization bits. The scenario has a BS equipped with M=2 antennas and K=2 single antenna UTs. The main parameters used in the simulations are based on LTE standard and for details see [40]. The number of quantization bits for b is set to 4, 5 and 6, which corresponds to the values of $B = 2bM$ equal to 16, 20 and 24, respectively. Despite the higher complexity and computational effort to perform the large codebooks ($N_c > N_s$), RVQ presents slightly better performances than UQ. The differences between both strategies become smaller as the number of quantization bits increases, since the curves tend to the perfect CSI feedback case.

Chapter 3

Millimeter Waves and Massive MIMO

In this third chapter, the millimeter waves and massive MIMO are described in more detail, explaining why they will be part of the future of 5G systems. A channel model using millimeter waves is presented.

3.1 Millimeter Waves

Nowadays practically all mobile communication are done in the 300 Mhz-3 GHz range of the spectrum, but with the increase of mobile data growth and the request for better capacity, reliability and throughput, this spectrum range, already so crowded, does not offer conditions to fulfill these desires [41] [42]. The current 4G systems are close to theoretical limits in terms of data rate per cell. So the use of a millimeter-wave band defined as a 30-300 GHz range can be the answer to those requirements. 5G may leverage the large bandwidth available at millimeter wave frequencies to provide gigabit-per-second data rate in outdoor wireless systems [43].

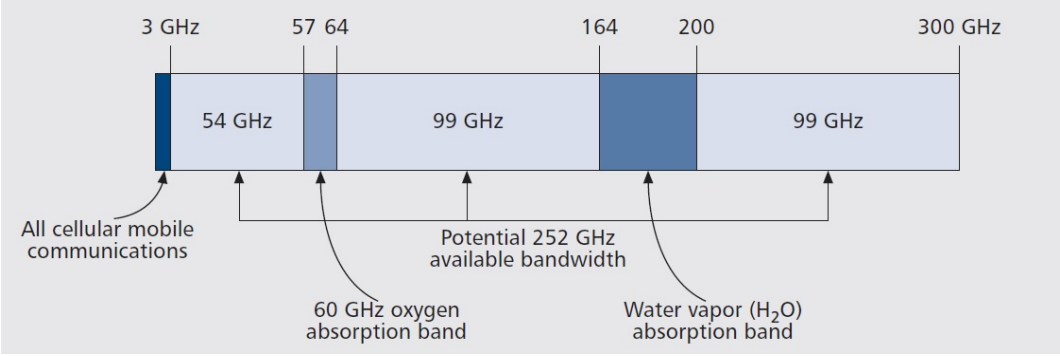

Figure 3.1: Millimeter Wave spectrum [12]

Thanks to the advancements of silicon and compound semiconductor technologies, has

become possible utilizing millimeter-wave frequencies [44]. Generally millimeter wave corresponds to the radio spectrum between 30-300 GHz, but in the wireless communication context, the term generally corresponds to a few bands of spectrum near 38, 60, 70, 90 and 94 GHz [45]. however this kind of waves have peculiar propagation characteristics, especially toward non-line-of-sight regions [41]. mmWave signals experience orders-of-magnitude more pathloss than microwave signals currently used in most wireless applications [46]. As they propagate through the atmosphere, the radio signals, are reduced in intensity by constituents of the atmosphere. Usually it happens in form of absorption or scatering, and dictates how much of the transmitted signal makes it to a cooperative receiver and how much of it gets lost in the atmosphere. The propagation characteristics of millimeter waves through the atmosphere depend primarily on atmospheric oxygen, humidity, fog and rain [45]. For example, in the 60 GHz band the signal loss due to atmospheric oxygen is significant, but in the 70 and 80 GHz bands is almost negligible. The loss of signal due to humidity and fog varies and depend on the quantity and size of liquid water droplets in the air, the loss can be at top 3dB/km. In comparison, the signal loss due to rain are much more significant. The Table 3.1 shows signal loss through atmosphere at 70 GHz.

Effect	**Comments**	**Signal Loss(dB/km)**
Oxygen	Sea Level	0.22
Humidity	100% at $30°C$	1.8
Heavy Fog	$10°C$, $1gm/m^3$	2.2
Cloud Burst	25 mm/hr rain	10.7

Table 3.1: Signal Loss through Atmosphere [45]

The signal loss due to rain depends on the rate of rainfall, as it may be concluded with Table 3.2.

Description	**Rain Rate**	**Signal Loss(dB/km)**
Light Rain	1mm/hour	0.9
Moderate Rain	4 mm/hour	2.6
Heavy Rain	25 mm/hour	10.7
Intense Rain	5 mm/hour	18.4

Table 3.2: Signal Loss due to Rain [45]

Although weather influence the signal loss, the performance of a millimeter wave link depends on other factors, such as diversity of redundant paths, distance between radio nodes and link margin of the radios [45].

3.2 Massive MIMO

After being proposed in 1993 and 1994 [47], MIMO technology is nowadays accepted as one of key technologies in Fouth Generation wireless communications systems [48]. For the

past years it matured and now the LTE standards allow for up 8×8 antenna systems, and it is known, basically the more antennas are equipped at transmitter and receiver, the more degrees of freedom(DoF) the channel can provide, the better performance in terms of data rate or link reliability without additional increase in bandwidth or transmit power [49] [50].

In a effort to achieve more dramatic gains, as well as reach all the benefits of conventional MIMO, massive MIMO systems have been proposed in [51] [52] (also known as large-scale antenna systems, very large MIMO, hyper MIMO, full-dimension MIMO, and ARGOS), which envisions the use of more antennas (e.g 100 or more) at each BS [38] [53]. A mMIMO system is capable of improving bandwidth efficiency and simultaneously reduce the transmit power [48]. It has also the potential to increase the capacity 10 times or more and improve the radiated energy efficiency on the orders of 100 times [13]. These multiplexing gains when serving tens of UTs simultaneously, and the large number of antennas help focus the energy with an extreme sharpness and narrow beam into small regions where the UTs are located [48] [13]. This extremely narrow beam can also reduce the Inter-User Interference(IUI).

Massive MIMO is a game changing technology, since it permits to replace the expensive ultra-linear 50W amplifiers used in conventional systems by hundreds of low-cost amplifiers with output power in the milli-Watt range. Several expensive items such as coaxial cables, can be eliminated. mMIMO reduces the constraints on accuracy and linearity of each individual amplifiers and RF chain. In a way, mMIMO count on the law of large numbers so noise, fading and hardware imperfections average out when signals from a large number of antennas are combined in the air, which also makes mMIMO extremely robust to failure of one or a few of antenna units [13].

Traditional MIMO systems can only adjust signal transmission in the horizontal dimension, make use of linear Antenna Array (AA). In order to exploit the vertical dimension of signal propagation, AAs such as rectangular, spherical and cylindrical AAs can be used. Figure 3.2 illustrate those antenna arrays. Linear AA as an example of Two-Dimensional (2D) AAs, and spherical AA, cylindrical AA and rectangular AAs as 3D antenna arrays. With this 3D arrays, both azimuth and elevation gains can be adjusted and propagate signals in Three-Dimensional space. Nowadays in an active AA, the RF circuit and the AA are integrated into a single circuit board, which is an important milestone in the development of antenna arrays. The distributed AA is mainly used inside buildings or for outdoor cooperation, while linear AA is mostly assumed in theoretical analysis and realistic measurements [48].

Having a good channel knowledge, on both uplink and downlink is important in massive MIMO. In the uplink case, the solution is having the terminals send pilots based on which the BS estimates the channel response to each of the terminals. On the downlink is more difficult. Since sending pilot waveforms, based on which the terminals estimate the channel responses, quantize the thus obtained estimates, and feed them back to the base station, is not feasible in massive MIMO as it is in conventional MIMO systems. First, optimal downlinks pilots should be mutually orthogonal between antennas, so the amount of time-frequency resources needed for downlink pilots scales with the number of antennas. Second the number of channel responses each terminal must estimate is also propotional to the number of base

stations antennas [13].

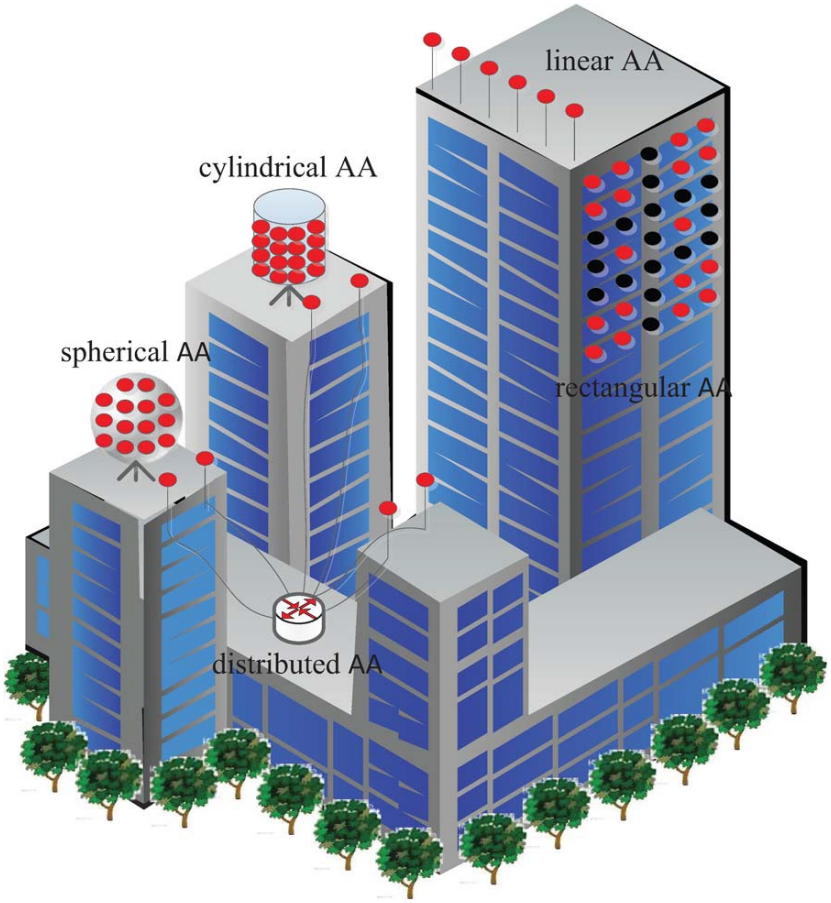

Figure 3.2: Different Antenna Arrays configurations [48]

3.3 Millimeter-Wave Massive MIMO

The combination of millimeter-wave communications, arrays with a massive number of antennas, and small cell geometries is a symbiotic convergence of technologies that has the potential to dramatically improve wireless access and throughput. Individually, each of these approaches could offer an order of magnitude increase in wireless capacity or more compared to current broadband systems; in combination with one another, one can envision achieving the approximate thousand-fold increase in capacity that will be needed in the coming decades [53].

In order to use the millimeter-wave band more efficiently, and attenuate the losses due to weather conditions, reflection and diffraction, various technologies are considered for use in 5G mobile communication networks. The decrease in wavelength enables packing a large number of antennas into small form factors. A massive antenna structure for forming multiple

beams can support spatial reuse of a base station. Large arrays can provide beamforming technology to improve the spectral efficiency of mobile communication networks, overcome pathloss and establish links with reasonable SNR. The beamforming technology also facilitates spatial reuse of limited radio resources in mobile communication networks [41] [46].

3.3.1 Antenna Designs

Historically, mmWave bands were ruled out for cellular usage mainly due to concerns regarding short-range and non-line-of-sight coverage issues. Although mmWave presents problems, also permits, due to low wavelength, reduce the dimension of the antennas and assemble a large number of antennas in the same space. Figure 3.3 show two schematics of antennas, one represent a single antenna working at 3 GHZ and the other an array of antennas working at 30 GHZ.

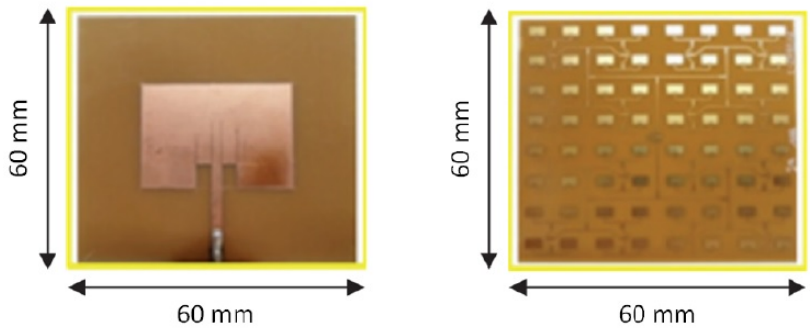

(a) Single Antenna 3 GHz (b) Array Antennas 30 GHz

Figure 3.3: Different Antenna Designs [54]

Although there is a common misunderstanding, that at higher frequencies the propagation loss increases, based on Friis equation. However high frequencies increase the path loss, increasing the number of antennas can compensate the losses. The test made in [54] [55–59] shows the potential of millimeter-wave massive MIMO systems.

Space constraint appears to be a engineering challenge at mmWave frequencies. The antenna elements in an array must be placed closely together to prevent grating lobes [60]. This implies that each antenna cannot be large compared to the wavelength, but also not too small and isotropic since some gain is needed to overcome the large path loss [53]. For example, at 72 GHz frequency, the required element spacing is only about 2 mm. With the current monolithic microwave integrated circuits (MMIC) technology, the practical implementation of such a digital antenna array remains very difficult.

A main problem of the use of conventional MIMO architecture in a mMIMO implementation is the need to replicate multiple transmit/receive chains, one for each antenna. Figure 3.4

shows a array antenna with 128 elements. Figure3.4 (a) use 4x4 RF chips (brown squares), each with 8 antennas in the package (yellow squares) because the insertion loss to bring the signal off-chip to an antenna would be too high and can be implemented at very high frequencies. The solution of Figure 3.4 (b) use 4x4 RF chips, each with 8 antennas mounted nearby on a circuit board or on a different substrate, and its used for lower frequencies, because at lower frequencies, the antennas are larger and not completely integrable within the chip package. Figure3.4 (c) shows the block diagram of the RF frontend with both TX and RX channels integrated in the chip connected to 8 antennas [53].

As was said previously full digital implementation of large, wideband antenna array at mmWave frequencies is unrealistic. A pure digital beamformer have excessive demand on real time signal processing for high gain antennas, for example, to achieve an antenna gain of over 30 dB, for instance, one may need more than 1000 antenna elements, making it impractical. Furthermore, to perform wideband digital beamforming, each signal from/to an antenna element is normally divided into a number of narrowband signals and processed separately, which also adds to the cost of digital signal processing significantly [43]. To solve the complexity of the digital implementation an hybrid adaptive antenna array is proposed in [60].

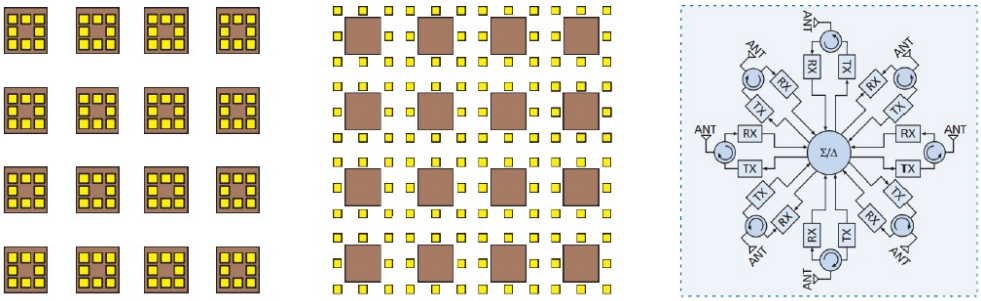

(a) High Frequencies (b) Lower Frequencies (c) Block diagram of the RF

Figure 3.4: Antenna Front-End Integration [53]

In a hybrid antenna array, a large number of antennas are grouped into analogue subarrays. Each subarray uses an analogue beamformer to produce beamformed subarray signal, and all subarray signals are combined using a digital beamformer to produce the final beamformed signal. Each element in a subarray has its own RF chain and employs an analogue phase shifting device at the intermediate frequency (IF) stage. Signals received by all elements in a subarry are combined after analogue phase shifting, and the analogue beamformed signal is down-converted to base band and then converted into digital domain. In this way, the complexity of the digital beamformer is reduced by a factor equal to the number of elements

in a subarray [60].

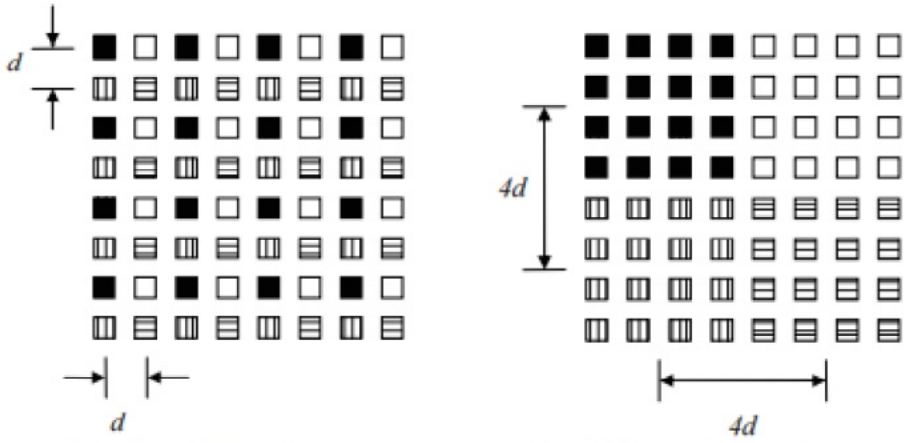

Figure 3.5: Hybrid Antenna Array [60]

3.3.2 Millimeter-Wave massive MIMO Architectures

With the use of mmWaves systems, precoding/combining is generally different than precoding at lower frequencies due to hardware constrains. The small wavelength of mmWave signals allows a large number of antennas to be packed into a small form factor, which translate in a increase of high cost and power consumption components like high-resolution analog-to-digital converters (ADCs), and it is difficult to dedicate a separate a RF chain with these components for each antenna. The large number of antennas also impacts the channel estimation and equalization. So with all the hardware constrains, different channel conditions and larger bandwidth, new architectures are needed for mmWave-mMIMO systems [61].

In order to around this constrains, new transceiver architectures such as hybrid analog/digital precoding (and combining), and the use of low resolution ADCs to reduce the power consumption at the receiver, have been discussed.

In the hybrid solution the precoding and beamforming are divided between the analog and digital domains. Via analog beamforming, the number of transceivers can be lowered towards the total antenna number. Each transceiver is connected with multiple active antennas, and the signal phase on each antenna is controlled via a network of analog phase shifters. The digital precoding layer adds more freedom for precoding compared to a pure analog beamforming solution, so digital beamforming can be utilized on top of analog BF, to achieve better performance [61] [62].

The solutions using low-resolution ADCs, can reduce the power consuption at the receiver. Low-resolution ADCs consume less power and at low SNR incur only a little rate loss compared

to high-resolution ADCs. Both approaches can coexist in the same system [61].

3.3.3 Hybrid analog/digital precoding

Two hybrid BF structures are shown in Figure 3.6, the full-array architecture and the sub-array architecture, with M_t being the transceiver number and M_r the number of active antennas per transceiver.

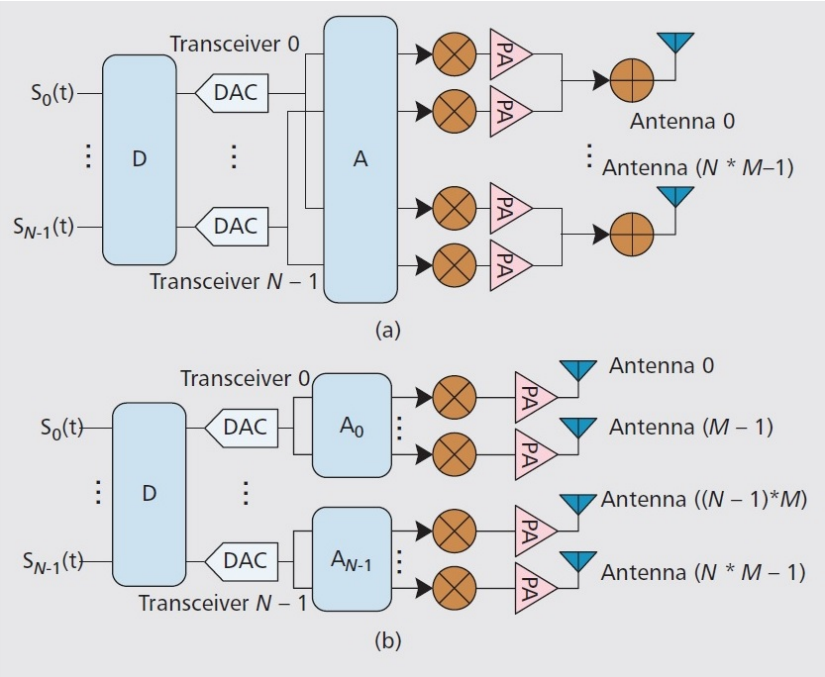

Figure 3.6: Hybrid precoding structures [62]

Figure 3.6(a) illustrates an architecture, where each transceiver is connected with all antennas, just as the transmitted signal on each of the M_t digital transceivers goes through $M_t \times M_r$ RF paths (mixer, power amplifier, phase shifter, etc.) and summed up before being connected with each antenna element. Then, analog BF is performed over $M_t \times M_r$ RF paths per transceiver, and digital BF can then be performed over M_t transceivers. This architecture can achieve full beamforming gain, but the complexity of this structure is quite high, as the total number of RF paths is $M_t^2 M_r$. With this structure, for mmWave communication, is used a simple precoding solution assuming only partial channel knowledge at the base station and mobile station in the form of angle of arrival (AoA) and angle of departure (AoD) knowledge [62].

A second structure is shown in Figure 3.6(b), where each of the M_t transceivers is connected to M_r antennas. Analog BF is performed over only M_r RF paths in each transceiver, and digital BF is performed over M_t transceivers. This structure is more practical for base

station antenna deployment in the current cellular systems, where each transceiver is generally connected to a column of antennas. With mmWave communication, this second structure use AoA estimation and beamforming algorithms [62].

3.3.4 1-bit ADC architecture

As previously said, a solution to overcome the limitation on the number of complete RF chains is to perform analog beamforming using networks of phase shifters. In mmWave systems, the sampling rate of the ADCs scales up with the larger bandwidth unfortunately high-resolution ADCs are costly and power-hungry. This turns out to be a problem for mmWave mMIMO systems. One possible solution, can be the use of low-resolution ADCs (1-3 bits), which reduces power consumption and cost. This structure has the advantage that the ADC can be implemented by a single comparator resulting in very low power consumption so as to simplify aspects of circuit complexity [61].

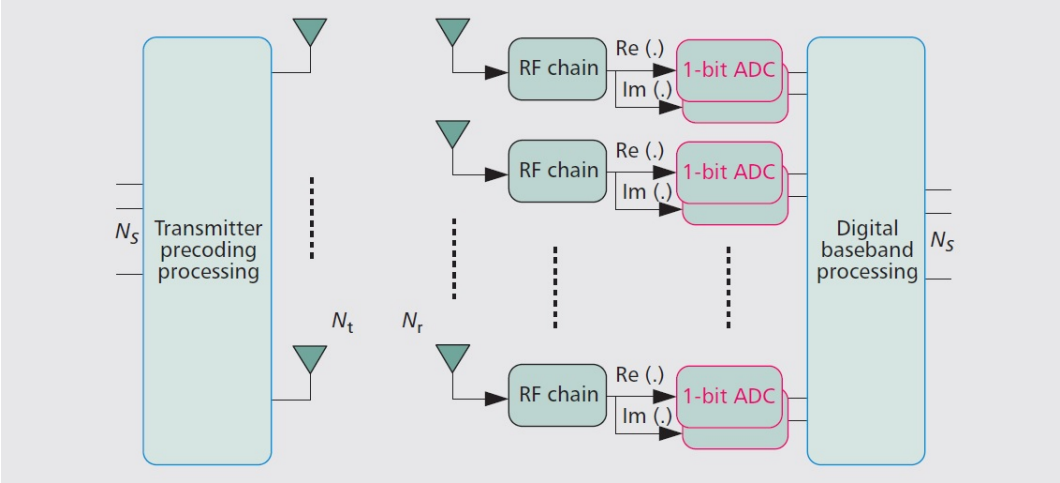

Figure 3.7: 1-bit ADC precoding structure [61]

3.4 Millimeter-Wave MIMO Channel Model

As it has being said in this dissertation, millimeter wave communications is a promising technology for the future cellular systems due to its huge bandwidth and small wavelength. The small wavelength of the millimeter wave (relative to the microwave) ensures that large-sized arrays can be implemented with a small form factor. As a result, mmWave systems provides sufficient array gain using large-sized array antennas and analog beamforming and combining at the base station and the mobile station [63] [64]. However, the mmWave MIMO channel is sparce due to propagation characteristics. High free-space pathloss leads to limited spacial selectivity or scatering, and the large tightly-packed antenna arrays leads to high antenna correlation. For these reasons, statistical fading distributions used in traditional

MIMO analysis are inaccurate for mmWave channel modeling [46]. Therefore channel models for mmWave communications have been discussed in [65–68].

In this section, it is briefly described the clustered mmWave channel model presented in [46].

Consider a single-user mmWave system with M_t transmit antennas and M_r receive antennas. The system have N_{cl} scattering cluster, and each one with N_{ray} propagation paths. Therefore, the discrete-time narrowband channel $\mathbf{H}$ can be written as:

$$\mathbf{H} = \gamma \sum_{n,l} \alpha_{nl} \Lambda_r(\phi^r_{nl}, \theta^r_{nl}) \Lambda_t(\phi^t_{nl}, \theta^t_{nl}) \mathbf{a}_r(\phi^r_{nl}, \theta^r_{nl}) \mathbf{a}_t(\phi^t_{nl}, \theta^t_{nl})^*, \tag{3.1}$$

where γ is a normalization factor such that $\gamma = \sqrt{M_t M_r / N_{cl} N_{ray}}$. The α_{nl} is the complex gain of the l^{th} ray in the n^{th} scattering cluster, while $\phi^r_{nl}(\theta^r_{nl})$ and $\phi^t_{nl}(\theta^t_{nl})$ are its azimuth (elevation) angles of arrival and departure respectively. α_{nl} follow a complex Gaussian distribution $\mathcal{CN}(0, \sigma^2_{\alpha,n})$ where $\sigma^2_{\alpha,n}$ represents the average power of the n^{th} cluster. The transmit and receive antenna element gain at the corresponding angles of departure and arrival are represented by $\Lambda_t(\phi^t_{nl}, \theta^t_{nl})$ and $\Lambda_r(\phi^r_{nl}, \theta^r_{nl})$. The azimuth angles of arrival and departure, are represented as θ^r_{nl} and θ^t_{nl} respectively [69]. Is assumed that α_{nl} have Gaussian distribution, are i.i.d. $\mathcal{CN}(0, \sigma^2_{\alpha,n})$ where $\sigma^2_{\alpha,n}$ represents the average power of the nth path. The average powers are such that $\sum_{n=1}^{N_{cl}} \sigma^2_{\alpha,n} = \gamma$ where γ satisfies $\mathbb{E}[||\mathbf{H}^2_F||] = M_t M_r$. The angles of arrival and departure, θ^r_{nl} and θ^t_{nl}, follow a Laplacian distribution.

Those array response vectors depends on the array antenna type. For an N-element Uniform Linear Array (ULA) on the y-axis, the array response vector is,

$$\mathbf{a}_{ULA_y}(\phi) = \frac{1}{\sqrt{N}} [1, e^{jkd\sin(\phi)}, ..., e^{j(N-1)kd\sin(\phi)}]^T, \tag{3.2}$$

where $k = \frac{2\phi}{\lambda}$, d is the inter-element spacing, $0 \leq m < N_y$ and $0 \leq n < N_z$.

In the case of a Uniform Planar Array, in the yz-plane with N_y and N_z elements on the y and z axes respectively, the array response vector is,

$$\mathbf{a}_{UPA}(\phi) = \frac{1}{\sqrt{N}} [1, ..., e^{jkd(m\sin(\phi)\sin(\theta) + n\cos(\theta))}, ..., e^{jkd((N_y-1)\sin(\phi)\sin(\theta) + (N_z-1)\cos(\theta))}]^T, \tag{3.3}$$

3.5 Advanced Small Cells

In the future 5G networks, it is desired to provide a multi-gigabit-per-second-based data rate for communication by using massive MIMO and mmWaves. The increase of the data rates can be processed by using mmWaves spectrum, and the smaller millimeter wavelength can be integrated with directional antennas for higher throughput because massive MIMO as a spatial processing technique can provide orthogonal polarization and beamforming adaptation. 5G networks will be highly dense networks, so in order to increase the efficiency, low-cost architectures called dense HetNet's or advanced small cells surge [70].

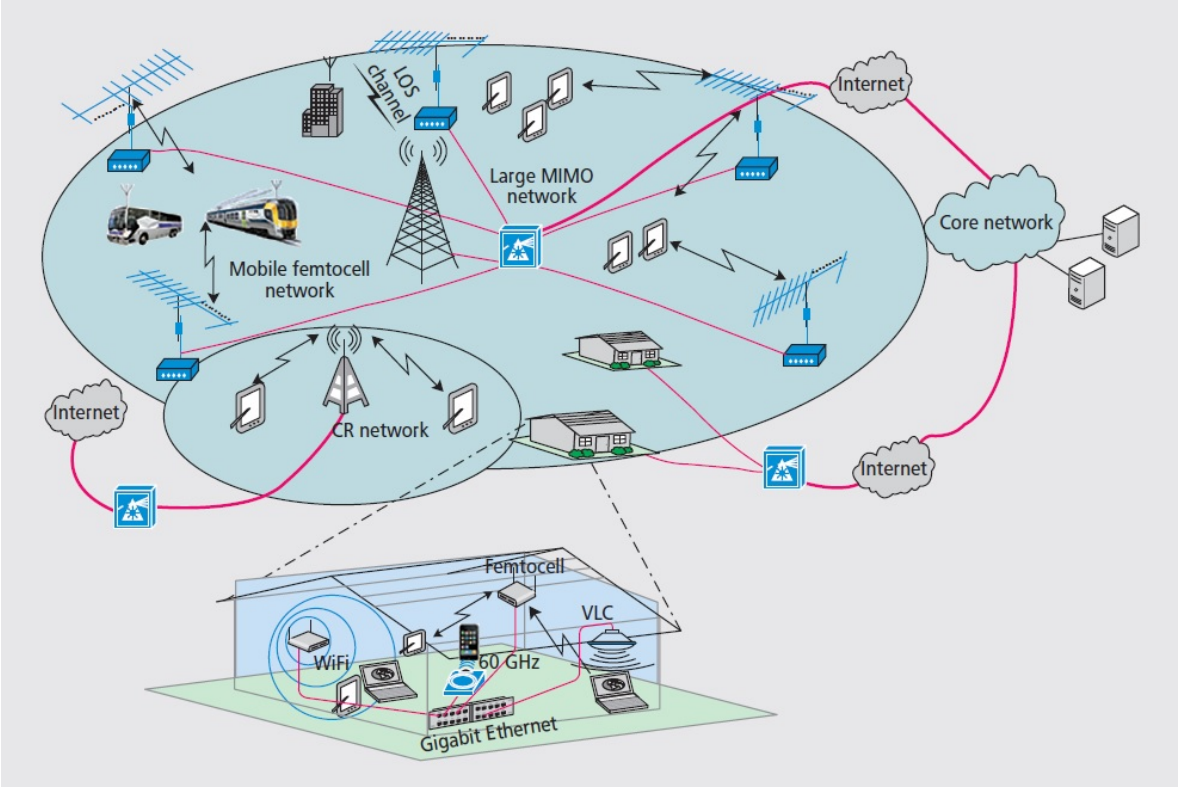

Figure 3.8: Heterogeneous wireless cellular architecture example [71]

It is believed that small cells will play a very important role in 5G to meet the 5G requirements in traffic volume, frequency effiency, and energy and cost reduction. A natural way to improve network capacity is to place further transmitters with moderate numbers of antennas at typical outdoor hotspot locations. More cells yield higher capacity if the frequencies are reused. High-speed data coverage is improved, and the network diversity is increased. Shorter distances between base stations and terminals and a higher line-of-sight probability are further benefits. Deployment of small cells indoors will probably use more powerful enhanced wireless local area networks to overcome the strong outdoor-to-indoor

penetration loss. Also less cooperation between indoor and macrocells is needed [72].

In 5G HetNets, macro and small cells may be connected to each other via ideal or non-ideal backhaul, resulting in different levels of coordination across the network for mobility and interference management. Increasing degrees of network cooperation, from loose network node coordination to completely centralized control, will provide increasing levels of network capacity. When access to ideal backhaul is not available, anchor-booster architecture may be used to coordinate between macro and small cells. In this architecture, the macro cell operates as an anchor base station, and is primarily responsible for control and mobility, while the small cell operates as a booster base station and is mainly responsible for offloading data traffic. The separation of data and control plane in anchor-booster architecture eases the integration of other RATs (Radio Access Technologies), such as WiFi or mmWave RATs, as booster cells within the LTE framework.

If the small cells can be connected to macrocells with low latency high-rate backhaul, the baseband signals from several hundred cells can be received and processes at centralized server platform. This architecture creates a super base station with distributed antennas supporting multiple RAN (Radio Access Network) protocols and dynamically adapting its signal processing resouses based on the varying traffic load within its geographical coverage. This architecture saves on operational cost by locating all the processing of multiple base station in one unit, and simplifies implementation of LTE-Advanced features such as coordinated multipoint (CoMP) and enhanced inter cell interference coordination (eICIC) by centralizing baseband processing [73].

D2D (Devide-To-Device) communication serves as another "cell tier" in the 5G HetNet, where clusters of devices cooperate with each other to dramatically increase network capacity. D2D communication enables the exchange of data traffic directly between user equipment without the use of base stations or core network other than for assistance in setting up direct connections. These type of communication supports new usage models based on the proximity of users, including social networking applications, peer-to-peer content sharing, and public safety communications in the absence of network coverage. They also confer additional benefits beyond increased area spectral efficiency, including improved cellular coverage, reduced end-to-end latency, and reduced power consumption [73].

HetNets are among the most promising low-cost approaches to meet the industry's capacity growth needs and deliver a uniform connectivity experience. Today's 3G and 4G networks are designed primarily with a focus on peak rate and spectral efficiency improvements. In the 5G Era, will be seen a shift towards network efficiency with 5G systems based on dense HetNet architectures.

Chapter 4

Hybrid mMIMO mmWave Systems Under Limited CSI

As mentioned before, the use of beamforming at transmitter side requires the knowledge of channel state information prior to transmission. The knowledge of the CSI can then be used to improve the performance in the downlink. However, assuming a perfect CSIT, is not realistic in many practical scenarios. Considering the particular case of mmW mMIMO based systems this problem is more significant since the terminals are equipped with a large number of antennas and therefore a huge amount of channels needed to be feedback from the receiver to the transmitter increasing the overall system signaling.

In this Chapter a single-user mmW massive MIMO system is evaluated under limited feedback. We consider a transmitter employing a hybrid analog-digital beamforming and a receiver equipped with an iterative hybrid analog-digital equalizer. Firstly, the implemented mmW massive MIMO platform is presented. Then, a low-overhead uniform quantization strategy is proposed, where only some channel parameters, such as the fading coefficients and phases. Finally, the system is evaluated under this CSI quantization strategy and compared with the case where perfect CSIT is known.

4.1 Hybrid mmWave mMIMO Platform

4.1.1 System Model

In this section, the mmWave mMIMO system used for this work is described, based in a hybrid architecture. Assuming a single-user mmWave system with M_t transmit antennas and M_r receive antennas, where the transmitter sends N_s data streams to the receiver, per time-slot. The channel remains constant during a block, with size T, but varies independently between blocks. The received signal for each block is given by,

$$\mathbf{Y} = \mathbf{HX} + \mathbf{N}, \tag{4.1}$$

where $\mathbf{Y} = [\mathbf{y}_1, ...\mathbf{y}_T] \in \mathbb{C}^{M_r \times T}$ denotes the received signal matrix, $\mathbf{X} = [\mathbf{x}_1, ..., \mathbf{x}_T] \in \mathbb{C}^{M_t \times T}$ is the transmitted signal, $\mathbf{N} = [\mathbf{n}_1, ..., \mathbf{n}_T] \in \mathbb{C}^{M_r \times T}$ is a zero mean Gaussian noise with

variance σ_n^2, and $\mathbf{H} \in \mathbb{C}^{M_r \times M_t}$ is the channel matrix.

In order to accurately model a mmWave channel, that combines tightly packed antenna arrays in sparce scattering environments, the channel model considered follows the clustered sparce mmWave channel model discussed in [74], given by the sum of the contributions of N_{cl} clusters, each of which contribute N_{ray} propagation paths to the channel matrix $\mathbf{H}$. The discrete-time narrowband channel is expressed as

$$\mathbf{H} = \gamma \mathbf{A}_r \Lambda \mathbf{A}_t^H, \tag{4.2}$$

where γ is a normalization factor such that

$$\gamma = \sqrt{\frac{M_t M_r}{N_{cl} N_{ray}}}, \tag{4.3}$$

Λ is a diagonal matrix defined as

$$\Lambda = \begin{bmatrix} \alpha_{1,1} & 0 & 0 & 0 & 0 \\ 0 & \alpha_{1,2} & 0 & 0 & 0 \\ 0 & 0 & \alpha_{2,1} & 0 & 0 \\ 0 & 0 & 0 & \ddots & 0 \\ 0 & 0 & 0 & 0 & \alpha_{N_{cl},N_{ray}} \end{bmatrix}, \tag{4.4}$$

with entries $n = 1, ..., N_{cl}$ and $l = 1, ..., N_{ray}$ that correspond to the paths gains of the lth ray in the nth scattering cluster. $\mathbf{A}_t$ and $\mathbf{A}_r$ are the matrices of array response vectors at the transmitter and receiver, formed by

$$\mathbf{A}_t = [\mathbf{a}_t(\theta_{1,1}^t), ..., \mathbf{a}_t(\theta_{N_{cl},N_{ray}}^t)], \tag{4.5}$$

and

$$\mathbf{A}_r = [\mathbf{a}_r(\theta_{1,1}^r), ..., \mathbf{a}_r(\theta_{N_{cl},N_{ray}}^r)], \tag{4.6}$$

respectively, whereas θ_{nl}^r and θ_{nl}^t are the azimuth angles of arrival and departure [69]. The array response vectors for a N_v element uniform linear array is given by

$$\mathbf{a}_v(\theta_{n,l}^v) = \frac{1}{\sqrt{N_v}}[1, e^{jkdsin(\theta_{n,l}^v)}, ..., e^{j(N_v-1)kdsin(\theta_{n,l}^v)}]^T, \tag{4.7}$$

with $v \in \{r, t\}$, $k = 2\pi/\lambda$ and d is the inter-element spacing [75].

Figure 4.1 shows the transmitter side of the hybrid based architecture used in this dissertation, and proposed in [69]. The transmitter processing consists in a digital baseband and analog circuitry parts. These two parts are modeled by precoders matrices, $\mathbf{F}_a \in \mathbb{C}^{M_t \times M_t^{RF}}$ for the analog part and $\mathbf{F}_d \in \mathbb{C}^{M_t^{RF} \times N_s}$ for digital part. There are M_t^{RF} transmit chain in

the digital part, with $N_s \leq M_t^{RF} \leq M_t$. Due to hardware constrains, the analog part is implemented using a matrix of analog phase shifters which force all elements of matrix $\mathbf{F}_a$ to have equal norm ($\mathbf{F}_a(i,l)^2 = M_t^{-1}$). The total power constraint of the transmitter is given by $||\mathbf{X}||_F^2 = N_s T$.

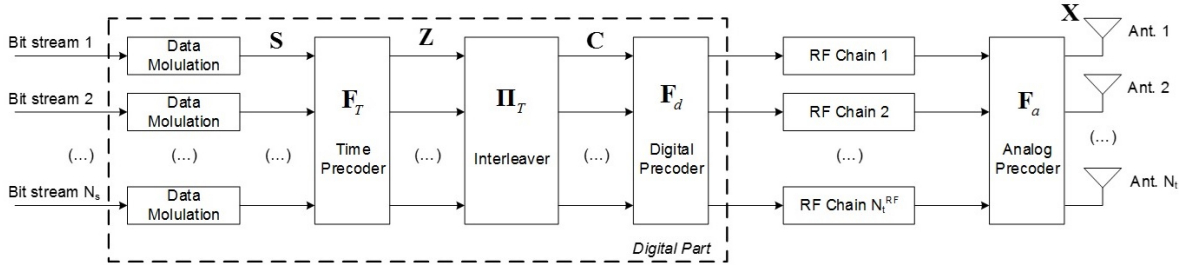

Figure 4.1: Transmitter block diagram [69]

After the digital part and the analog circuitry, the transmit signal is given by

$$\mathbf{X} = \mathbf{F}_a \mathbf{F}_d \mathbf{C}, \tag{4.8}$$

where $\mathbf{C} = [c_1, ..., c_T] \in \mathbb{C}^{N_s \times T}$ denotes a codeword contructed by using a space-time block code. This STBC can be mathematically described by

$$\mathbf{z}_t = \mathbf{S}\mathbf{f}_t, \tag{4.9}$$

$$\mathbf{c}_t = \Pi_t \mathbf{z}_t, \tag{4.10}$$

where t=1,...,T denotes the time index, $\mathbf{f}_t \in \mathbb{C}^T$ denotes column t of a T point DFT matrix ($\mathbf{F}_T = [\mathbf{f}_1, ..., \mathbf{f}_T]$), $\Pi_t \in \mathbb{C}^{N_s \times N_s}$, t=1,...,T is a random permutation matrix known at the transmitter and receiver sides, and $\mathbf{S} = [s_{s,t}]_{1 \leq s \leq N_s, 1 \leq t \leq T} \in \mathbb{C}^{N_s \times T}$, with $s_{t,s}, t \in \{1, ..., T\}, s \in \{1, ..., N_s\}$ denoting a complex data symbol chosen from a QAM constellation with $\mathbb{E}[|s_{s,t}|^2] = \sigma_s^2$, where $\sum_{s=1}^{N_s} \sigma_s^2 = N_s$. However in this dissertation, to simplify and without loss of generality, only QPSK constellations are used. To compute the codeword $\mathbf{C}$, its applied and FFT transform to the rows of the symbol matrix $\mathbf{S}$ (Equation 4.9) and then permute each of the resulting T columns with a random permutation $\Pi_t, t1, ..., T$ (Equation 4.10).

At the receiver it was considered the hybrid iterative space-time decoder proposed in [69]and shown in Figure 4.2. First, the received signal is processed through the analog phase shifters, modeled by the matrix $\mathbf{W}_a \in \mathbb{C}^{M_r^{RF} \times M_r}$, then follows the baseband processing,

composed by M_r^{RF} processing chains. The elements of the matrix $\mathbf{W}_a$ must have equal norm ($|\mathbf{W}_a(j,l)|^2 = M_r^{-1}$).

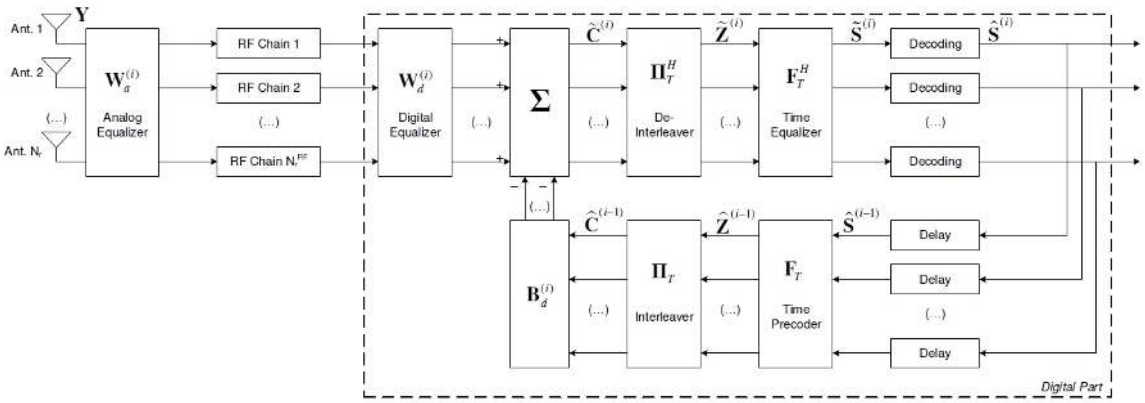

Figure 4.2: Receiver block diagram [69]

The baseband processing includes a digital feedback closed-loop. For the forward path of the closed-loop, the signal first passes through a linear filter $\mathbf{W}_d \in \mathbb{C}^{N_s \times M_r^{RF}}$, then follows the decoding of the STBC with demodulation included. In the feedback path, the data recovered in the forward path is first modulated and encoded using the STBC, then it passes through the feedback matrix $\mathbf{B}_d \in \mathbb{C}^{N_s \times N_s}$. The STBC decoding is given by

$$\tilde{\mathbf{Z}} = \left[\Pi_1^H \tilde{c}_1, ..., \Pi_T^H \tilde{c}_T\right], \tag{4.11}$$

$$\tilde{\mathbf{S}} = \tilde{\mathbf{Z}}\mathbf{F}_T^H, \tag{4.12}$$

To obtain a soft estimate of the transmitted symbols, first it is inverted the permutation applied at the transmitter (4.11), and then apply the IDFT transform to the resulting matrix, as in (4.12). The feedback and feedforward paths are combined by subtracting the signal output of the feedback path from the filtered received signal $\mathbf{W}_d\mathbf{W}_a\mathbf{Y}$.

4.1.2 Hybrid Precoder Design

Millimeter-wave precoders ($\mathbf{F}_a, \mathbf{F}_d$) are designed, in order to maximize the spectral efficiency. $\mathbf{F}_d \in \mathbb{C}^{M_T^{RF} \times N_S}$ is the digital precoder, and $\mathbf{F}_a \in \mathbb{C}^{M_T \times M_T^{RF}}$ is the analog precoder, both at the transmitter side. The transmitter has also M_T^{RF} RF chains and M_T antennas. Starting by examining the mutual information achieved by the hybrid precoders $\mathbf{F}_a\mathbf{F}_d$ the channels's optimal unconstrained precoder $\mathbf{F}_{opt}$ can be obtained. To do so, is defined the channel's ordered SVD to be $\mathbf{H} = \mathbf{U}\mathbf{\Sigma}\mathbf{V}^H$, where $\mathbf{U}$ is and $M_r \times rank(\mathbf{H})$ unitary matrix, $\mathbf{\Sigma}$ is a $rank(\mathbf{H}) \times rank(\mathbf{H})$ diagonal matrix of singular values arranged in decreasing order,

and $\mathbf{V}$ is a $M_r \times rank(\mathbf{H})$ unitary matrix. Beyond that, defining the matrices $\mathbf{\Sigma}$ and $\mathbf{V}$ as

$$\mathbf{\Sigma} = \begin{bmatrix} \mathbf{\Sigma}_1 & 0 \\ 0 & \mathbf{\Sigma}_2 \end{bmatrix}, \quad \mathbf{V} = \begin{bmatrix} \mathbf{V}_1 & \mathbf{V}_2 \end{bmatrix}, \tag{4.13}$$

where $\mathbf{\Sigma}_1$ have dimension $N_S \times N_S$ and $\mathbf{V}_1$ dimension $M_t \times N_S$. It can be noted that the optimal unconstrained unitary precoder for $\mathbf{H}$ is given by

$$\mathbf{F}_{opt} = \mathbf{V}_1, \tag{4.14}$$

$\mathbf{F}_{opt}$ have dimension $M_t \times N_S$ and is the requirement to start with the algorithm presented in Table 4.1 and proposed in [46], to achieve the desired precoders $(\mathbf{F}_a, \mathbf{F}_b)$.

Algorithm - Precoding	
Require: $\mathbf{F}_{opt}$	
1:	$\mathbf{F}_a$ = Empty Matrix
2:	$\mathbf{F}_{res} = \mathbf{F}_{opt}$
3:	**for** $i \leq M_t^{RF}$ **do**
4:	$\Psi = \mathbf{A}_t^H \mathbf{F}_{res}$
5:	$k = arg\,max_{l=1,\ldots,N_{c1}N_{ray}} (\Psi\Psi^H)_{l,l}$
6:	$\mathbf{F}_a = [\mathbf{F}_a | \mathbf{A}_t^{(k)}]$
7:	$\mathbf{F}_d = (\mathbf{F}_a^H \mathbf{F}_a)^{-1} \mathbf{F}_a^H \mathbf{F}_{opt}$
8:	$\mathbf{F}_{res} = \frac{\mathbf{F}_{opt} - \mathbf{F}_a \mathbf{F}_d}{||\mathbf{F}_{opt} - \mathbf{F}_a \mathbf{F}_d||_F}$
9:	**end for**
10:	$\mathbf{F}_d = \sqrt{N_S} \frac{\mathbf{F}_d}{||\mathbf{F}_a \mathbf{F}_d||_F}$
11:	**return** $\mathbf{F}_a$, $\mathbf{F}_d$

Table 4.1: Precoder Algorithm

The analog $\mathbf{F}_a \in \mathbb{C}^{M_t \times M_t^{RF}}$ matrix and the digital $\mathbf{F}_d \in \mathbb{C}^{M_t^{RF} \times N_S}$ are computed to minimize $||\mathbf{F}_{opt} - \mathbf{F}_a \mathbf{F}_d||_F^2$. It may be advantageous to impose the additional constraint that $\mathbf{F}_d$ be unitary. Unitary precoders can be more efficiently quantized and are thus more attractive in limited feedback systems. So in the algorithm described in Table 4.1 the step 7 is replaced by $\mathbf{F}_d = \hat{\mathbf{U}}\hat{\mathbf{V}}^H$, where $\hat{\mathbf{U}}$ and $\hat{\mathbf{V}}^H$ are unitary matrices defined by $\mathbf{F}_a^H \mathbf{F}_{opt} = \hat{\mathbf{U}}\hat{\mathbf{\Sigma}}\hat{\mathbf{V}}^H$. More details about this hybrid precoder algorithm can be found in [46].

4.1.3 Hybrid Receiver Design

In this section, it is briefly described the iterative space-time receiver proposed in [69] shown in Figure 4.2. At the ith iteration the received signal at the tth time slot, after the

de-interleaver, is given by

$$\tilde{\mathbf{z}}_t^{(i)} = \mathbf{\Pi}_t^H(\mathbf{W}_{d,t}^{(i)}\mathbf{W}_{a,t}^{(i)}\mathbf{y}_t - \mathbf{B}_{d,t}^{(i)}\mathbf{\Pi}_t\hat{\mathbf{z}}_t^{(i-1)}), \tag{4.15}$$

$$\hat{\mathbf{Z}}^{i-1} = \hat{S}^{i-1}\mathbf{F}_T, \tag{4.16}$$

where $\mathbf{\Pi}_t^H \in \mathbb{C}^{N_s \times N_s}$ denotes the de-interleaver matrix, $\mathbf{W}_{a,t}^{(i)} \in \mathbb{C}^{M_r^{RF} \times M_r}$ is the analog part of the feedforward matrix. The digital part is composed by the feedforward matrix, $\mathbf{W}_{d,t}^{(i)}$ and the feedback matrix $\mathbf{B}_{d,t}^{(i)}$. $\mathbf{\Pi}_t \in \mathbb{C}^{N_s \times N_s}$ is the interleaver and $\hat{\mathbf{Z}}^{i-1} = [\hat{\mathbf{z}}_1^{(i-1)}, ..., \mathbf{z}_T^{(i-1)}] \in \mathbb{C}^{N_s \times T}$ is the DTF of the detector output $\hat{\mathbf{S}}^{(i-1)}$. The matrix $\hat{\mathbf{C}}^{(i)} = [\mathbf{\Pi}_1\hat{\mathbf{z}}_1^{(i)}, ..., \mathbf{\Pi}_T\hat{\mathbf{z}}_T^{(i)}]$ denotes the hard estimate of the transmitted codeword $\mathbf{C}$ and $\hat{\mathbf{S}}^{(i)} = sign(\tilde{\mathbf{S}}^{(i)})$ the hard decision associated to QPSK data symbols $\mathbf{S}$, at iteration i. Through central limit theorem the entries of vector $\mathbf{z} : t$, $t \in \{1, ..., T\}$ are Gaussian distributed, then as the input-output relationship between variables $\mathbf{z}_t$ and $\hat{\mathbf{z}}_t^{(i)}$, $t \in \{1, ..., T\}$ is memoryless. Follows

$$\hat{\mathbf{z}}_t^{(i)} = \mathbf{\Psi}^{(i)}\mathbf{z}_t + \hat{\boldsymbol{\epsilon}}_t^{(i)}, \quad t \in \{1, ..., T\}, \tag{4.17}$$

where $\mathbf{\Psi}^{(i)}$ is a diagonal matrix given by

$$\mathbf{\Psi}^{(i)} = diag(\Psi_1^{(i)}, ...\Psi_s^{(i)}, ...\Psi_{N_s}^{(i)}), \tag{4.18}$$

$$\Psi_s^{(i)} = \frac{\mathbb{E}[\hat{\mathbf{z}}_t^{(i)}](s)\hat{\mathbf{z}}_t^*(s)}{\mathbb{E}[|\hat{\mathbf{z}}_t(s)|^2]}, \; s \in \{1, ..., N_s\}, \tag{4.19}$$

and $\hat{\boldsymbol{\epsilon}}_t^{(i)}$ is a zero mean error vector uncorrelated with $\mathbf{z}_t$, with $\mathbb{E}[\hat{\boldsymbol{\epsilon}}_t^{(i)}\hat{\boldsymbol{\epsilon}}_t^{(i)^H}] = (\mathbf{I}_{N_s} - |\mathbf{\Psi}^{(i)}|^2)\sigma_s^2$. It can be defined the vector

$$\mathbf{\Gamma}^{(i)} = \mathbf{T}^{-1}\sum_{t=1}^{T}(\mathbf{\Pi}_t^H\mathbf{W}_{d,t}^{(i)}\mathbf{W}_{a,t}^{(i)}\mathbf{H}\mathbf{F}_a\mathbf{F}_d\mathbf{\Pi}_t), \tag{4.20}$$

corresponding to the equivalent overall channel from signal $\mathbf{s}_t$ to $\tilde{\mathbf{s}}_t^{(i)}$, so

$$\tilde{\mathbf{s}}_t^{(i)} = \mathbf{\Gamma}^{(i)}\mathbf{s}_t + \tilde{\mathbf{e}}_t^{(i)}, \tag{4.21}$$

with $\tilde{\mathbf{e}}_t^{(i)} = \tilde{\mathbf{s}}_t^{(i)} - \mathbf{\Gamma}^{(i)}\mathbf{s}_t$ denoting an overall error that includes both the channel noise and the residual intersymbol interference (ISI). Since the vector $\hat{\mathbf{e}}_t^{(i)}$ is uncorrelated with $\mathbf{z}_t$, the average power is given by

$$\begin{aligned} MSE_t^{(i)} &= \mathbb{E}[||\tilde{\mathbf{z}}_t^{(i)} - \mathbf{z}_t||^2] \\ = \mathbb{E}[||\tilde{\boldsymbol{\epsilon}}_t^{(i)}||^2] &= ||(\mathbf{W}_{ad,t}^{(i)})\mathbf{H}_t - \mathbf{\Gamma}_t^{(i)} - (\mathbf{B}_{d,t}^{(i)})\mathbf{\Psi}^{(i-1)}||_F^2\sigma_s^2 \\ &+||(\mathbf{B}_{d,t}^{(i)})(\mathbf{I}_{N_s} - \mathbf{\Psi}^{(i-1)}|^2)^{1/2}||_F^2\sigma_s^2 + ||(\mathbf{W}_{ad,t}^{(i)})||_F^2\sigma_n^2, \end{aligned} \tag{4.22}$$

where $\mathbf{W}_{ad,t}$ represents a digital equalizer, i.e. in case each antenna has one RF chain. The receive analog and digital parts are jointly designed. The analog matrix $\mathbf{W}_{a,t}^{(i)}$ and the digital $\mathbf{W}_{d,t}^{(i)}$ and $\mathbf{B}_{d,t}^{(i)}$ are computed to minimize the mean-square-error (MSE) between the transmit and the receive signals given by (4.22). The derived algorithm is described in Table 4.2. More details about this algorithm can be found in [69].

Algorithm
Require: $(\overline{\mathbf{W}}_{ad,t}^{(i)})_{opt}$
$(\mathbf{W}_{a,t}^{(i)})_{opt}$ = Empty Matrix
$\mathbf{W}_{res,t}^{(i)} = -(\overline{\mathbf{W}}_{ad,t}^{(i)})_{opt}\tilde{\mathbf{R}}_t^{(i-1)}$
for $i \leq M_r^{RF}$ **do**
$k = arg\,max_{1,...,N_{cl}N_{ray}}(\mathbf{A}_r^H(\mathbf{W}_{res,t}^{(i)})^H\mathbf{W}_{res,t}^{(i)}\mathbf{A}_r)_{l,l}$
$(\mathbf{W}_{a,t}^{(i)})_{opt} = [((\mathbf{W}_{a,t}^{(i)})_{opt})^H \vert (\mathbf{A}_r^{(k)})]^H$
$(\mathbf{W}_{d,t}^{(i)})_{opt} = \mathbf{\Omega}_d((\mathbf{W}_{a,t}^{(i)})_{opt}\mathbf{H}_t)^H(\mathbf{R}_{d,t}^{(i-1)})^{-1}$
$\mathbf{W}_{res,t}^{(i)} = ((\mathbf{W}_{d,t}^{(i)})_{opt}(\mathbf{W}_{a,t}^{(i)})_{opt} - (\overline{\mathbf{W}}_{ad,t}^{(i)})_{opt})\tilde{\mathbf{R}}_t^{(i)} + \mathbf{U}_d(\mathbf{H}_t)^H$
end for
return $(\mathbf{W}_{a,t}^{(i)})_{opt}$, $(\mathbf{W}_{d,t}^{(i)})_{opt}$

Table 4.2: Hybrid Iterative Equalizer Algorithm

4.2 Millimeter-Wave Channel Quantization

The CSI is needed in both transmitter and receiver sides to compute the hybrid analog-digital precoders and equalizers. For the sake of simplicity we assume perfect channel estimation at the receiver side. The method for CSI estimation is out of this work. In practice, the channel can be estimated at the receiver through appropriate training sequences and/or pilots [74]. From the previous Section, we can see that to compute the analog-digital precoders, we need to know the matrix $\mathbf{H}$ and the transmit array response $\mathbf{A}_t$ as illustrated in Figure 4.3. More specifically, to compute the digital precoder we need to know the matrix $\mathbf{H}$ and to compute the analog precoder we need matrix $\mathbf{A}_t$, and thus this information should be fed back from the receiver to the transmitter. This would imply a quantization and feedback of $M_tM_r + M_tN_{ray}N_{cl}$ complex values per block (it is considered the channel constant during a block of size T).

In order to reduce the feedback overhead we propose to quantize and fed back just some parameters that are characteristic of the channel, followed by channel reconstruction in transmitter and precoder computation. It can be seen by (4.2) that the channel matrix $\mathbf{H}$ is composed by three main parts: the transmit array response, $\mathbf{A}_t$, the fading complex coefficients α_{nl}, with $n = 1, ..., N_{cl}$ and $l = 1, ..., N_{ray}$, and the receive array response, $\mathbf{A}_r$.

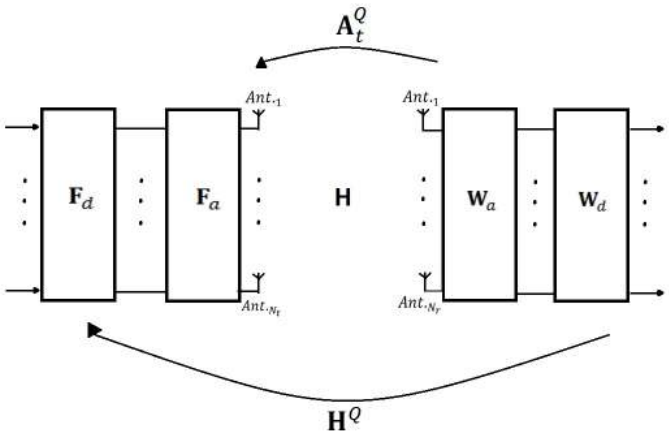

Figure 4.3: Hybrid System Model

Therefore, we quantize each of these parts individually, i.e., we propose to quantize uniformly the complex path gains $\alpha_{n,l}$, and the real values of the azimuth angles of arrival and departure $\theta^r_{n,l}$ and $\theta^t_{n,l}$, respectively, with $n = 1, ..., N_{cl}$ and $l = 1, ..., N_{ray}$, obtaining the quantized variables.

$$\alpha^Q_{n,l} = f_{Q\alpha}(Re\{\alpha_{n,l}\}) + jf_{Q\alpha}(Im\{\alpha_{n,l}\}), \tag{4.23}$$

$$\theta^r_{n,l}{}^Q = f_{Qr}(\theta^r_{n,l}), \tag{4.24}$$

$$\theta^t_{n,l}{}^Q = f_{Qt}(\theta^t_{n,l}), \tag{4.25}$$

$f_{Q\alpha}$, f_{Qr} and f_{Qt} are the quantization characteristic functions based on uniform quantization using b_α, b_r and b_t bits, respectively, and where the levels are equally spaced in $[-\alpha_c, \alpha_c]$, $[-\theta^r_c, \theta^r_c]$ and $[-\theta^t_c, \theta^t_c]$, respectively, with α_c, θ^r_c and θ^t_c being the clipping values for amplitude and azimuth angles of arrival and departure, respectively. For the azimuth angles of arrival and departure, the clipping values are given by one-half of the receiver and the transmitter sector angles, respectively. For the path gains, since the variable is not limited a previous study was done to observe which are the better clipping values for each b_α. Figure 4.5 has an example of an ideal clipping value for the amplitude path loss variable. Figure 4.4 shows the clipping characteristic function for α_c, where the variable to quantize is in the x-axis and the

clipped variable is in the y-axis.

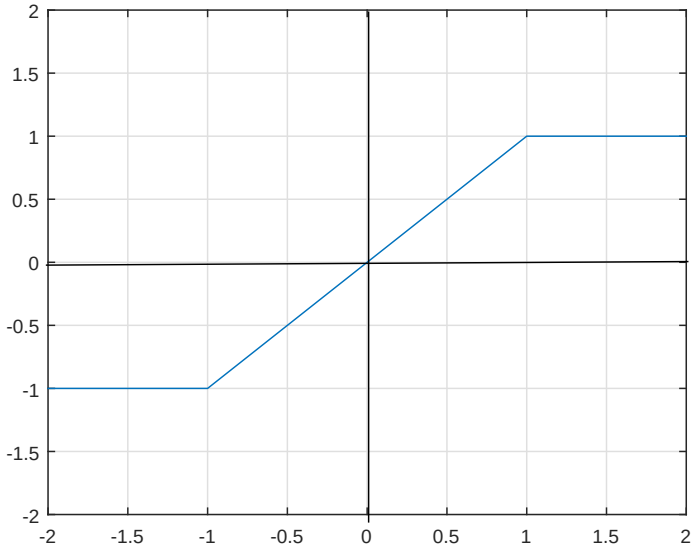

Figure 4.4: Clipping characteristic function for α_c=1

After quantization, these parameters are fed back to the transmitter, where they are then used to reconstruct the matrices of array response vectors of transmitter and receiver, defined as

$$\mathbf{A}_t{}^Q = [\mathbf{a}_t(\theta^t_{1,1})^Q, ..., \mathbf{a}_t(\theta^t_{N_{cl},N_{ray}})^Q], \tag{4.26}$$

and

$$\mathbf{A}_r{}^Q = [\mathbf{a}_r(\theta^r_{1,1})^Q, ..., \mathbf{a}_r(\theta^r_{N_{cl},N_{ray}})^Q], \tag{4.27}$$

respectively and the channel matrix is obtained through

$$\mathbf{H}^Q = \gamma \mathbf{A}_r{}^Q \Lambda^Q \mathbf{A}_t^{HQ}, \tag{4.28}$$

where

$$\Lambda^Q = \begin{bmatrix} \alpha_{1,1}{}^Q & 0 & 0 & 0 & 0 \\ 0 & \alpha_{1,2}{}^Q & 0 & 0 & 0 \\ 0 & 0 & \alpha_{2,1}{}^Q & 0 & 0 \\ 0 & 0 & 0 & \ddots & 0 \\ 0 & 0 & 0 & 0 & \alpha_{N_{cl},N_{ray}}{}^Q \end{bmatrix}, \tag{4.29}$$

To obtain the precoder matrix we start by assessing the $\mathbf{F}^Q_{opt}$ matrix, using $\mathbf{H}^Q$, as in (4.13). The quantized SVD channel is $\mathbf{H}^Q = \mathbf{U}^Q\mathbf{\Sigma}^Q\mathbf{V}^{HQ}$, so $\mathbf{F}^Q_{opt}$ is given by

$$\mathbf{F}_{opt}{}^Q = \mathbf{V}_1{}^Q, \tag{4.30}$$

Then, through the same algorithm described in Table 4.1, the final precoder matrices $\mathbf{F}_a^Q$ and $\mathbf{F}_d^Q$, are obtained using $\mathbf{A}_t^Q$

Algorithm - Precoding
Require: $\mathbf{F}_{opt}^Q$
$\mathbf{F}_a^Q$ = Empty Matrix
$\mathbf{F}_{res}^Q = \mathbf{F}_{opt}^Q$
for $i \leq M_t^{RF}$ **do**
$\Psi = \mathbf{A}_t^{HQ}\mathbf{F}_{res}^Q$
$k = arg\,max_{l=1,\ldots,N_{c1}N_{ray}}(\Psi\Psi^H)_{l,l}$
$\mathbf{F}_a^Q = [\mathbf{F}_a^Q \vert \mathbf{A}_t^{(k)Q}]$
$\mathbf{F}_d^Q = (\mathbf{F}_a^{HQ}\mathbf{F}_a^Q)^{-1}\mathbf{F}_a^{*Q}\mathbf{F}_{opt}^Q$
$\mathbf{F}_{res}^Q = \frac{\mathbf{F}_{opt}^Q - \mathbf{F}_a^Q\mathbf{F}_d^Q}{\vert\vert\mathbf{F}_{opt}^Q - \mathbf{F}_a^Q\mathbf{F}_d^Q\vert\vert_F}$
end for
$\mathbf{F}_d^Q = \sqrt{N_S}\frac{\mathbf{F}_d^Q}{\vert\vert\mathbf{F}_a^Q\mathbf{F}_d^Q\vert\vert_F}$
return $\mathbf{F}_a^Q$, $\mathbf{F}_d^Q$

Table 4.3: Precoder Algorithm

Note that the quantization of channel parameters will also affect the combining process in the receiver, being important to conclude about how the quantization errors affect the over all system performance.

4.3 Performance Results

In this section, we access the performance of the proposed hybrid space-time iterative equalizer. A clustered channel model with $N_{cl} = 8$ clusters, each cluster with $N_{ray} = 10$ rays is considered. Is assumed that $\alpha_{n,l}$ are i.i.d., $\mathcal{CN}(0, \sigma_{\alpha,n}^2)$, where $\sigma_{\alpha,n}^2$ defines the average power of the nth cluster. The average power of the all N_{cl} clusters is the same and such that $\sum_{n=1}^{N_{cl}} \sigma_{\alpha,n}^2 = \gamma$, where γ is the normalization factor in (4.3). The N_{ray} azimuth angles of departure and arrival within cluster n, $\theta_{n,l}^t$ and $\theta_{n,l}^r$, respectively, are assumed to follow a Laplacian distribution, with a uniformly-random mean cluster angle of θ_n^t and θ_n^r, and a constant angular spread σ_{θ^t} and σ_{θ^r}, respectively. The angle spread at both the transmitter and receiver is set to 8 degrees. We assume that the transmitter's sector angle is 60° wide in the azimuth domain and the receiver antenna array has omnidirectional antenna elements. Thus the clipping values for the azimuth angles are 30° and 180° for transmitter and receiver, respectively. The antenna element spacing is assumed to be half-wavelength. The channel remains constant during a block, with size $T = 32$ and takes independent values between blocks.

The performances are evaluated in terms of bit error rate, which is presented as function

of the E_b/N_0, with E_b denoting the average bit energy and N_0 the one-sided noise power spectral density. Is considered $\sigma_1^2 =, ..., \sigma_{N_s}^2 = 1$ and then the average E_b/N_0 is identical for all streams $s \in \{1, ..., N_s\}$.

The results were obtained for the scenario described in Table 4.4

	Data Symbols	**Transmitter Antennas**	**Receiver Antennas**	**Transmitter RF Chains**	**Receiver RF Chains**
Scenario	8	128	32	8	8

Table 4.4: Considered Scenario

As previously said, for amplitude Rayleigh fading components quantization, different values of clipping α_c could be used. These clipping values depends on the number of quantization bits used, b_α. Figure 4.5 shows the impact of the saturation level, α_c, and the number of quantization bits, b_α, on MSE. As it can be observed, there is an optimum normalized saturation level for each value of b_α. The quantizer's saturation becomes too frequent if α_c is small and the quantization interval becomes too high when α_c is high. Hereinafter, it is assumed always the optimum saturation level for each value of α_c.

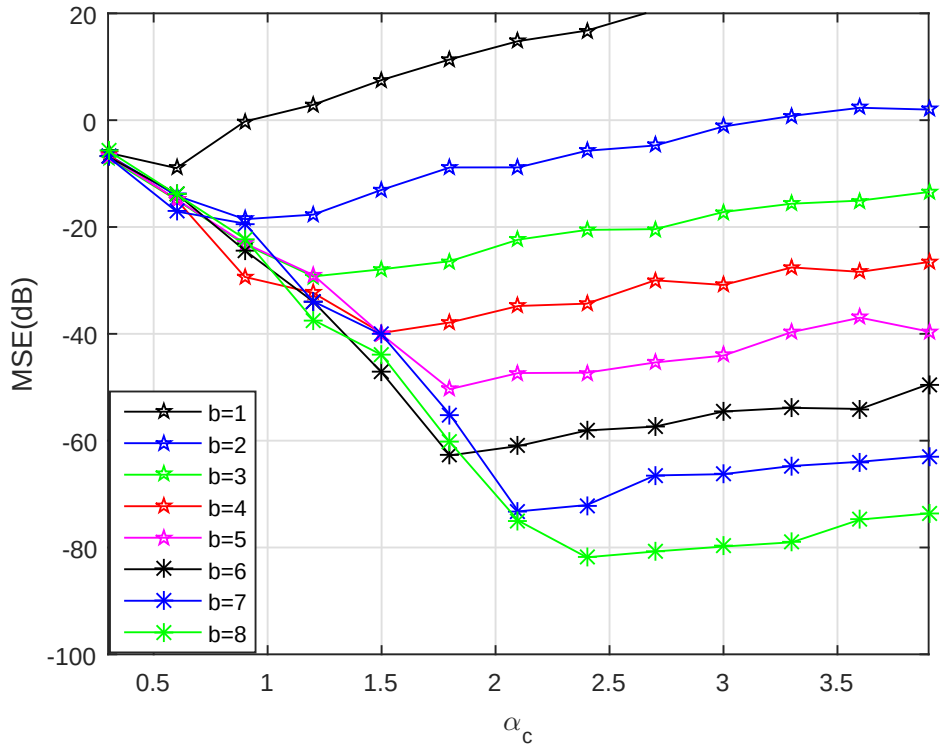

Figure 4.5: MSE curves for amplitude path gain quantization for different clipping values and number of quantization bits

Table 4.5 shows the optimal α_c for each quantization bit, b_α.

b_α	1	2	3	4	5	6	7	8
α_c	0.6	0.9	1.2	1.5	1.8	1.8	2.1	2.4

Table 4.5: Optimal α_c

Firstly, it is evaluated the impact on the performance of the transmit and receive arrays response $\mathbf{A}_t$ and $\mathbf{A}_r$, respectively. Therefore, to obtain these first results α_{nl} is assumed to be perfect. The results are always compared with perfect channel, i.e. assuming perfect knowledge of $\mathbf{A}_t$, $\mathbf{A}_r$ and α_{nl} at the transmit side. The results presented from Figure 4.6 to Figure 4.10 were obtained for one iteration of the considered iterative hybrid analog-digital equalizer, while for Figure 4.11 4 iteration was used.

Figure 4.6 shows the results for the channel reconstructed with perfect α_{nl} and $\mathbf{A}_t$. In this scenario only $\mathbf{A}_r^Q$ is quantized. In Figure 4.7 is depicted the results for channel reconstructed with perfect α_{nl} and $\mathbf{A}_r$. Here only $\mathbf{A}_t^Q$ is quantized. The aim is to understand the individual impact of $\mathbf{A}_r^Q$ and $\mathbf{A}_t^Q$ on the system performance. Finally, Figure 4.8 shows the impact for the case where both transmit array response $\mathbf{A}_t^Q$ and receive array response $\mathbf{A}_r^Q$ are quantized. In this last figure it is also assumed that the amplitudes α_{nl} are perfect.

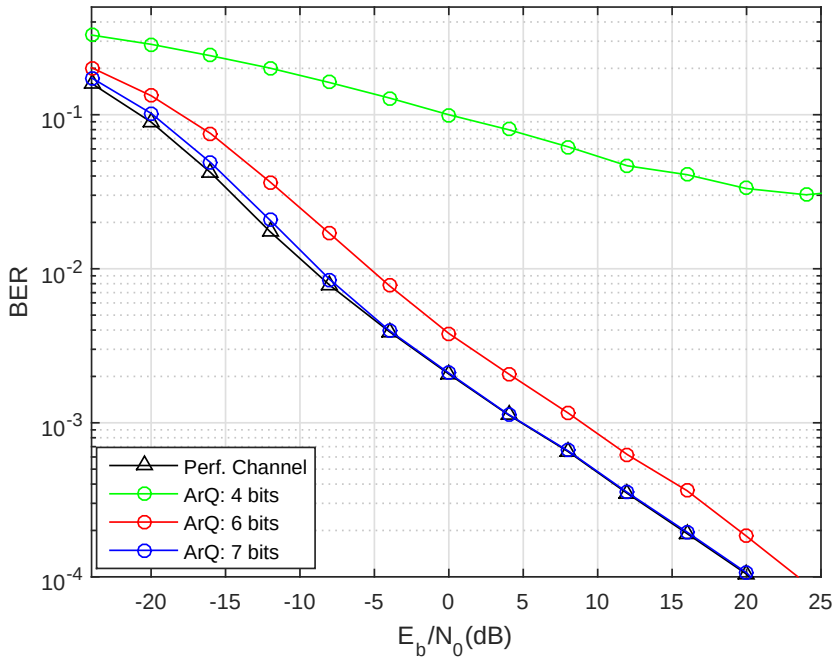

Figure 4.6: BER for hybrid mmWave mMIMO for perfect path gains and azimuth angles of departure, with quantized azimuth angles of arrival

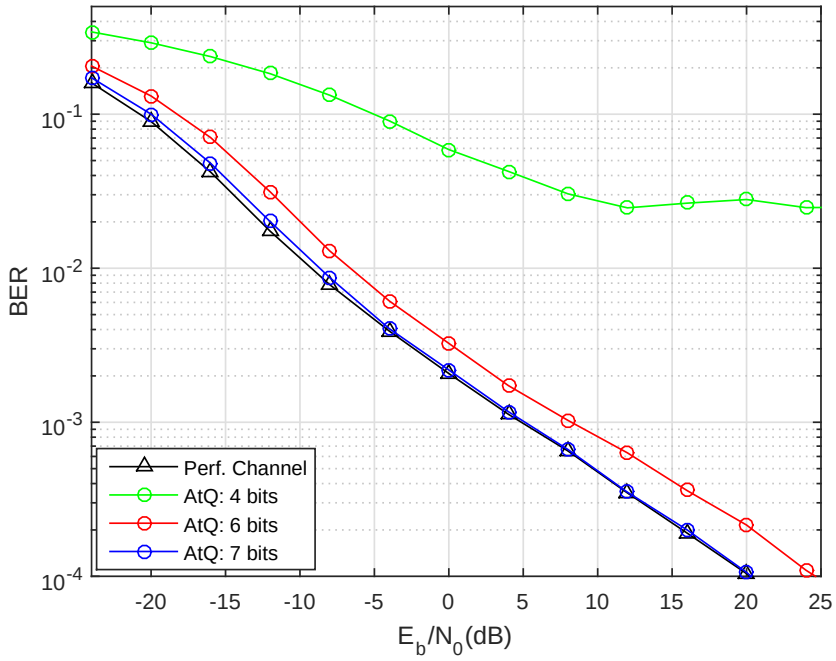

Figure 4.7: BER for hybrid mmWave mMIMO for perfect path gains and azimuth angles of arrival, with quantized azimuth angles of departure

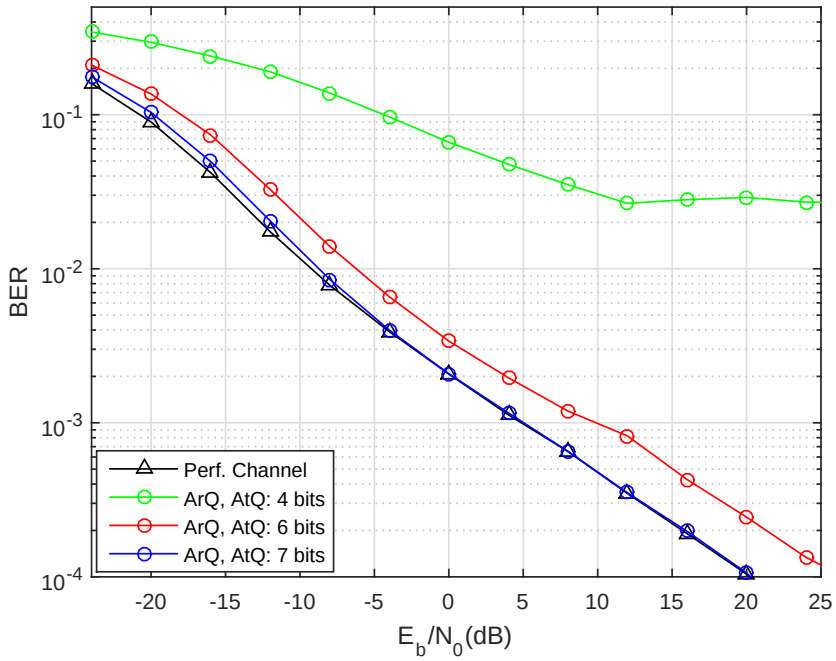

Figure 4.8: BER for hybrid mmWave mMIMO for perfect path gains, and quantized azimuth angles

It can be seen in these three previous figures, that the quantization of both azimuth angles, of arrival and departure, or just one of them has few influence in the system performance. However the results are slightly better when just quantizing the departure angles, which can be justified by the lower transmitter sector angle. It is important to observe that the higher the number of quantization bits the better are the results, as it is expected. It is possible to observe that with 7 bits, the performance result with quantization is almost juxtaposed to the curve with perfect channel state information.

Now the channel reconstruction is performed by assuming that all parameters, amplitudes and transmit and receive array responses are quantized, in order to have an overall picture. In Figure 4.9, α_{nl} is quantized with 2 bits while in Figure 4.10, 3 quantization bits were used. Comparing Figure 4.9 with Figure 4.10, the difference from using 2 or 3 bits to quantize those paths is visible, mainly for lower values of E_b/N_0. There is no need to use more bits for path gains since the curve obtained with $b_\alpha = 3$ and $b_r = b_t = 7$ almost perfectly match to the perfect channel one. This means that the amplitudes quantization have less impact on system performance. The quantization of transmit and receive array responses play a more important role on the feedback strategies design.

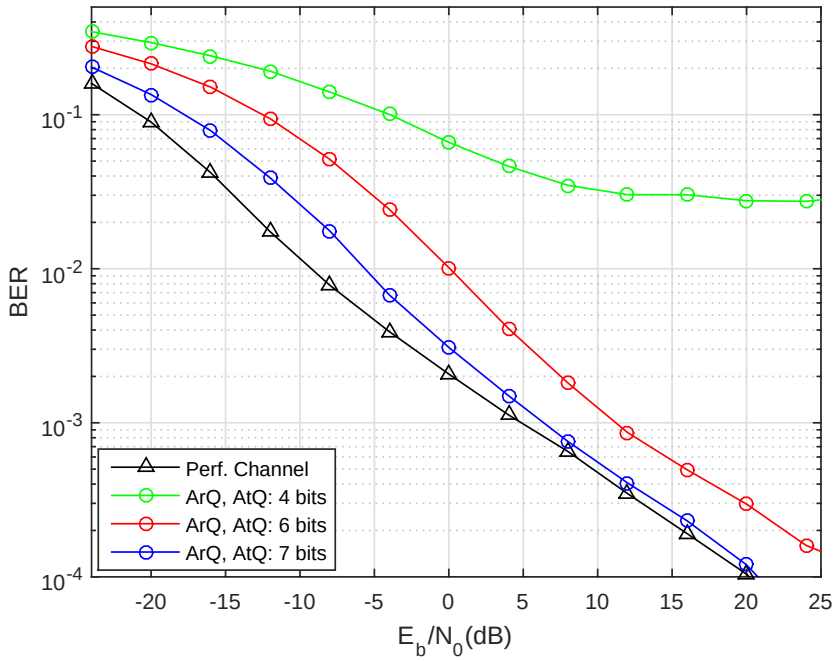

Figure 4.9: BER for hybrid mmWave mMIMO for quantized path gains with 2 bits, and quantized azimuth angles

Figure 4.11 show the BER results for the same conditions used in Figure 4.10 ($b_\alpha = 3$) but now for 4 iterations. It can be seen that the performance is better than with only 1 iteration. Again a high number of quantization bits translates in better results, and with 4 iteration the curves decay faster and are closer to each others.

Thus it can be seen that in order to achieve good results, is important to use a proper number of quantization bits. From the figures 4.6-4.8 it can be seen that the gap between the perfect channel curve and the 4 bit BER curve is substantial. Using perfect path gains and quantize the azimuth angles with 4 bits is not enough to achieve good results. Using 6 and 7 bits the results are much better, with the gap between curves becoming smaller. With 7 bits, the curve is almost equal to the perfect one. When all the parameters are quantized, the results show that the path gain need less quantization bits than the azimuth angles. It was also shown that using 4 iterations will bring better results.

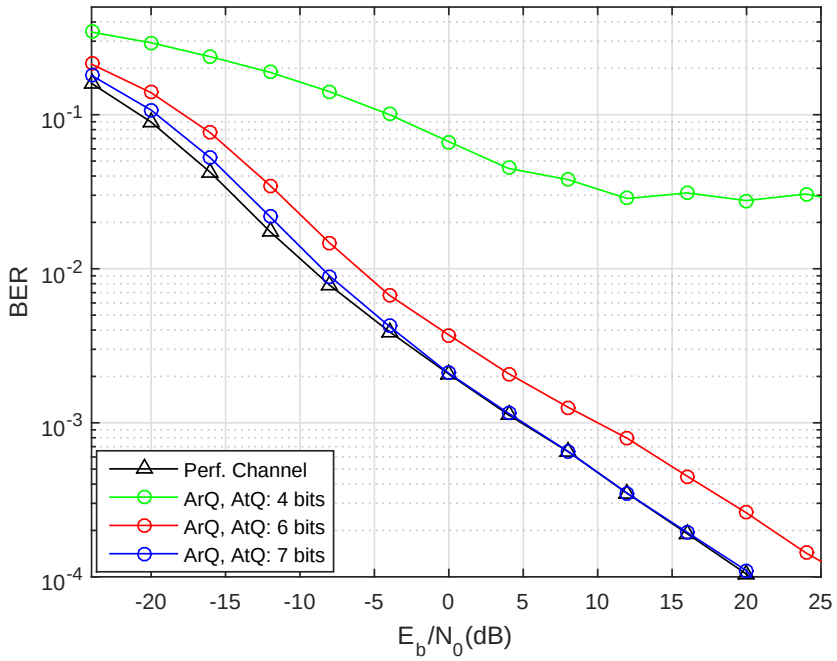

Figure 4.10: BER for hybrid mmWave mMIMO for quantized path gains with 3 bits, and quantized azimuth angles

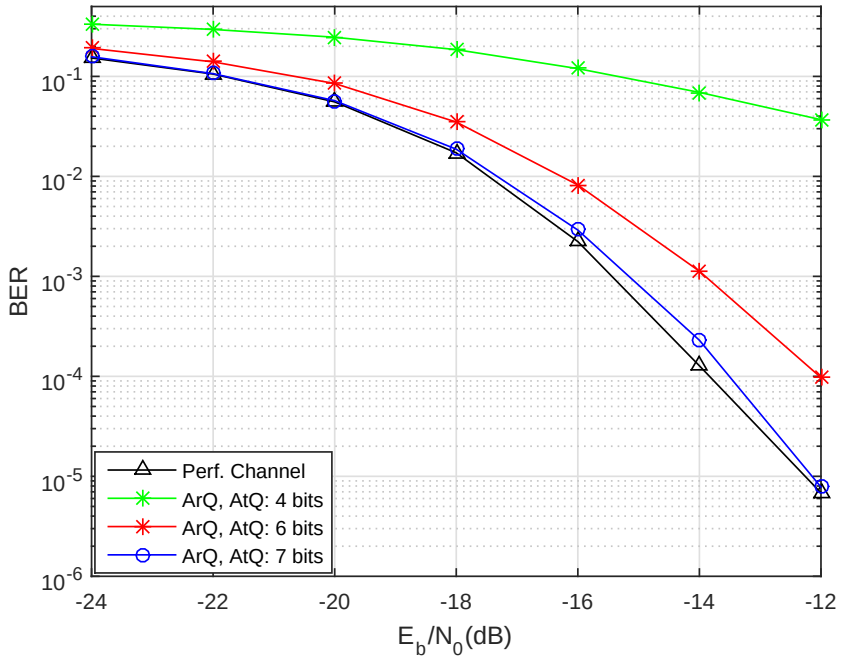

Figure 4.11: BER for hybrid mmWave mMIMO for quantized path gains with 3 bits, and quantized azimuth angles with 4 iterations

Chapter 5

Conclusions and Future Work

The mobile proportion of internet use has increased rapidly, in 2012 that proportion was about 40%, 68% in 2016, and some forecasts points to 75% in 2017. The rise of mobile internet use, challenges the creation of systems capable of responding to the demands of this increase. As 4G systems are reaching it capacities, 5G systems are being studied and designed. Two key technologies for future 5G systems, are millimeter-waves and massive MIMO. Although improving the bit rate and system capacity, these technologies result in many challenges to solve. The knowledge of the CSI at the transmit side to perform beamforming is an important step to have good and reliable wireless transmissions. The work presented in this dissertation helped to understand how the channel feedback process can be applied to hybrid architecture for mmWave mMIMO systems that require CSIT knowledge.

5.1 Conclusions

This dissertation started by a briefly presentation of the evolution of cellular communications, from the first generation to the forthcoming 5th generation. Since the use of mobile phones will keep growing, as they will serving for more services such as being abble to do payements or communicate with home appliences, 5G is an important system to future communications.

In Chapter 2 it was shown how multiple antenna systems can allow to have better performance and data rates. Techniques such as diversity, multiplexing and beamforming were discussed. In this chapter it was also introduced the principles of channel quantization and two ways to do it, the Random Vector Quantization and the Uniform Quantization. It was concluded that RVQ is not a feasible technique due to the complexity of the codebook for mMIMO systems.

Follow up, in Chapter 3 two key technologies that will make part of the 5G systems were described, the mmWave and mMIMO. Additionally millimeter-Wave massive MIMO systems were introduced, describing the antenna design for these systems and some possible architectures. Hybrid architectures process the signal in the analog and digital domain separately. Single user hybrid architectures have shown good performances. Also, in this chapter it was

presented a clustered mmWave channel model.

In Chapter 4 a single-user mmW massive MIMO system was evaluated under limited feedback. It was considered a transmitter employing a hybrid analog-digital beamforming and a receiver equipped with an iterative hybrid analog-digital equalizer. It was started by presenting the mmW massive MIMO platform implemented. Then, a low-overhead uniform quantization strategy was described in detail, where only some channel parameters, such as the fading coefficients, phases and delays were quantized. Finally, the system was evaluated under this CSI quantization strategy and compared with the case of perfect CSI. As the overall conlusion it can be said that imperfect CSI has a strong impact on hybrid mMIMO mmW bases systems as expected and the proposed quantization strategy is quite efficient, achieving a performance close to the one obtained with perfect CSI with a low number of quantization bits. Some specific conclusions can be pointed out:

- Increasing the number of quantized bits, the performance tends to the perfect CSI as expected.
- Imperfect knowledge of the transmit and receive array responses has stronger impact on the system performance that the complex channel amplitudes. This is expected since the beamforming is manly computed based on the knowledge of arrays response.
- It was shown that it is only need about 6-7 bits to efficiently quantize the transmit and receive arrays responses, $\mathbf{A}_t$ and $\mathbf{A}_r$, respectively. Both have approximately the same impact on the system performance.
- The complex amplitudes, α_{nl}, have less impact on the system performance and it was shown that 2-3 bits are perfectly enough to achieve a performance close case of perfect CSI.

5.2 Future Work

Regarding future work further studies can be done such as,

- Implement and compare other channel quantization strategies recently proposed for mmW mMIMO systems
- Apply this technique to quantize the channel parameters in other mmW mMIMO architectures.
- It also would be interesting to extend the considered quantization strategy for multi-user mmW mMIMO systems.

Bibliography

[1] Ankita Jain, Arjun Rajput,Subhra Dixit, "Evolution of Wireless Communication", [Available online] http://www.ijetsr.com/images/short_pdf/1429291482_ankita_ijetsr_(2).pdf

[2] Pankaj Sharma, "Evolution of Mobile Wireless Communication Networks-1G to 5G as well as Future Prospective of Next Generation Communication Network", [Available online] http://d.researchbib.com/f/annJcwp21wYzAioF9xo2AmY3OupTIlpl9OqJq1p3DlZQRmY1LlFGtlZQRmZGphpTEz.pdf

[3] E. Dahlman, S. Parkvall, J. Skold and P. Beming, *3G Evolution: HSPA and LTE for Mobile Broadband*, Elvesir Ltd., 1st edition, 2007.

[4] M. L. Roberts, M. A. Temple, R. F. Mills and R. A. Raines, "Evolution of the Air Interface of Cellulares Communications Systems Toward 4G Realization", *IEEE Communications Surveys & Tuturials*, vol. 8, no. 1, 2006.

[5] Apurv Modi "Millimeter wave mobile communication for 5G cellular", [Available online] http://www.slideshare.net/APURVAPPAY/millimeter-wave-mobile-communication-for-5g-cellular

[6] GSMA "The Mobile Economy 2016", [Available online] www.gsma.com/mobileeconomy/

[7] E. Dahlman, S. Parkvall, J. Skold, *4G: LTE/LTE-Advanced for Mobile Broadband*, Elvesir Ltd., 2nd edition, 2014.

[8] C. Cox, *An Introduction to LTE*, Chichester: John Wiley & Sons Ltd, 2012.

[9] Theodore S. Rappaport, Shu Sun, Rimma Mayzus, Hang Zhao, Yaniv Azar, Kevin Wang, George N. Wong, Jocelyn K. Schulz, Mathew Samimi, and Felix Gutierrez, "Millimeter Wave Mobile Communications for 5G Cellular: It Will Work!", *IEEE Access*, vol.1, pp. 335-349, May 2013.

[10] Federico Boccardi, Robert W. Heath Jr., Angel Lozano, Thomas L. Marzetta, Petar Popovski, "Five Disruptive Technology Directions for 5G", *IEEE Communications Magazine*, pp. 74-80, February 2014.

[11] Emil Björnson "Radio Resource Management in Massive MIMO Communication Systems", [Available online] http://www.commsys.isy.liu.se/en/research/projects/CENIIT-Radio-Resource-Management

[12] Zhouyue Pi and Farooq Khan, Samsung Electronics, "An Introduction to Millimeter-Wave Mobile Broadband Systems", *IEEE Communications Magazine*, pp. 101-107, June 2011.

[13] Erik G. Larsson, Ove Edfors and Fredrik Tufvesson, Thomas L. Marzetta, "Massive MIMO for Next Generation Wireless Systems", *IEEE Communications Magazine*, pp. 186-195, February 2014.

[14] Chun Kin Au-Yeung, David J. Love, "On the Performance of Random Vector Quantization Limited Feedback Beamforming in a MISO System", *IEEE Transactions on Wireless Communications*, vol. 6, No. 2, pp. 458-462, February 2007.

[15] S. Teodoro, A. Silva, R. Dinis, and A. Gameiro, "Low bit rate feedback strategies for iterative IA-precoded MIMO-OFDM based systems", *The Scientific World Journal*, vol. 2014, Article ID 619454, 11 pages, Feb. 2014.

[16] Lizhong Zheng, "Diversity and Multiplexing: A Fundamental Tradeoff in Multiple Antenna Channels", *IEEE Transactions On Information Theory*, vol. 49, No. 5, pp. 1073-1096, May 2003.

[17] Graham Celine, Azimuth Systems "LTE vs. WiMAX – A Test Perspective", [Available online] `https://abm-website-assets.s3.amazonaws.com/wirelessdesignmag.com/s3fs-public/legacyimages/1006/wd1006_Azimuth1_lrg.jpg`

[18] Ian Poole, Mimo formats - siso, simo, miso, mu-mimo. [Available online at] `http://www.radio-electronics.com/info/antennas/mimo/formats-siso-simo-miso-mimo.php`

[19] Gustavo Anjos, "MIMO Processing Techniques for 4G Systems", Master's thesis, Universiade de Aveiro, 2013.

[20] Claude Oestes, Bruno Clerckx *MIMO Wireless Communications: From Real-World Propagation to Space-Time Code Design*, Elsevier Ltd. 2007.

[21] Andreas F. Molisch *Wireless Comunications* John Wiley & Sons Ltd. 2011.

[22] K. Fazel, S. Kaiser, *Multi-Carrier and Spread Spectrum Systems* John Wiley & Sons Ltd. 2008.

[23] Raqibul Mostafa, Ramesh C. Pallat, Uwe Ringel, Ashok A. Tikku, and Jeffrey H. Reed, "Closed-Loop Transmit Diversity Techniques for Small Wireless Terminals and Their Performance Assessment in a Flat Fading Channel", *ETRI Journal*, vol. 34, no. 3, June 2012.

[24] Siavash M. Alamouti "A Simple Transmit Diversity Technique for Wireless Communications", *IEEE Journal on select areas in communications*, vol. 16, no. 8, pp. 1451-1458, October 1998.

[25] Vahid Tarokh "Space–Time Block Codes from Orthogonal Designs", *IEEE Transactions on information theory*, vol. 45, no. 5, pp. 1456-1467, July 1999.

[26] Hamid Jafarkhani "A Quasi-Orthogonal Space–Time Block Code", *IEEE Transactions on communications*, no. 1, vol. 49, pp. 1-4, January 2001.

[27] O. Tirkkonen, A. Boariu, A. Hottinen, "Minimal nonorthogonality rate one spacetime block codes for 3+ Tx antennas", in *IEEE ISSTA conference*, USA, 2000.

[28] A. Silva and A. Gameiro "Multiple Antenna Systems", University of Aveiro: Comunicações Sem Fios Lecture, 2015/16.

[29] [Available online] `http://www.oocities.org/hamsadhwani8/smartantennas/diversity.html`

[30] Farooq Khan, *LTE for 4G Mobile Broadband: Air Interface Technologies and Performance*, Cambridge University Press 2009.

[31] [Available online] `http://www.multicap.be/en/technology/mimo-and-spatial-streams`

[32] A. Sibille, C. Oestges and A. Zanella, *MIMO From Theory to Implementation*, Academic Press, 2011.

[33] [Available online] `http://ee.princeton.edu/research/prucnal/content/broadband-adaptive-photonic-beamforming?destination=node/191`

[34] I. E. Telatar, "Capacity of multi-antenna Gaussian channels" *Europ. Trans. Telecomm.*,vol. 10, no. 6, pp. 585-595, 1999 .

[35] G. J. Foschini and M. J. Gans, "On limits of wireless communications in a fading environment when using multiple antennas", *Wireless Personal Communications*, vol. 6, pp. 311-335, Mar. 1998.

[36] A. Scaglione, P. Stoica, S. Barbarossa, G. B. Giannakis, and H. Sampath, "Optimal designs for space-time linear precoders and decoders",*IEEE Trans. Signal Processing*, vol. 50, no. 5, pp. 1051-1064, May 2002.

[37] A. Narula, M. J. Lopez, M. D. Trott, and G. W. Wornell, "Eficient use of side information in mulitiple-antenna data transmission over fading channels", *IEEE Jour. Select. Areas in Commun.*, vol. 16, no. 8, pp. 1423-1436, Oct. 1998.

[38] D. J. Love, R. W. Heath Jr., V. K. N. Lau, D. Gesbert, B. D. Rao, and M. Andrews "An overview of limited feedback in wireless communication systems", *IEEE J. Sel. Areas Commun.*, vol. 26, no. 8, pp. 1341-1365, 2008.

[39] W. Santipach and M. L. Honig, "Asymptotic capacity of beamforming with limited feedback", *Proc. IEEE Int. Symp. Spread Spectrum Tech. and Appl.*, June-July 2004, p. 290.

[40] S. Teodoro, A. Silva, R. Dinis, and A. Gameiro, "Robust iterative interference alignment with limited feedback", in *Proc. of IEEE GLOBECOM Workshops 2015*, San Diego (CA), USA, Dec. 2015.

[41] Jun Suk Kim, Jae Sheung Shin, Sung-Min Oh, Ae-Soon Park, Min Young Chung "System Coverage and Capacity Analysis on Millimeter-Wave Band for 5G Mobile Communication Systems with Massive Antenna Structure", *International Journal of Antennas and Propagation* Volume 2014 (2014), Article ID 139063, 11 pages, 2005.

[42] Nicholas P. Lawrence,Brian W.-H. Ng,Hedley J. Hansen, Derek Abbott "Analysis of millimeter-wave polarization diverse multiple-input multiple-output capacity", *Royal Society Open Science* 2(12):150322, December 2015.

[43] A. Alkhateeb, O. El Ayach, G. Leus, and R. W. Heath. "Hybrid precoding for millimeter wave cellular systems with partial channel knowledge", *Information Theory and Applications Workshop (ITA), 2013*, pages 1-5, Feb 2013.

[44] W. Hong, Y. G. Kim, K. h. Baek, and Y. Lee. "Design and testing of a millimeter-wave beam-steering mesh-grid array for 5th generation (5g) mobile communication handset devices", *Radio Science Meeting (Joint with AP-S Symposium), 2014* USNC-URSI, pages 282-282, July 2014 .

[45] Prasanna Adhikari. "Understanding millimeter wave wireless communication", *VP of Business Development for Network Solutions, Loea Corporation, San Diego*, 2008.

[46] Omar El Ayach, Sridhar Rajagopal, Shadi Abu-Surra, Zhouyue Pi, and RobertWHeath. "Spatially sparse precoding in millimeter wave MIMO systems", *Wireless Communications, IEEE Transactions on*, 13(3):1499-1513, 2014.

[47] T. Kailath, A.J. Paulraj, "Increasing capacity in wireless broadcast systems using distributed transmission/directional reception (dtdr)", September 6 1994. US Patent 5,345,599.

[48] Kan Zheng, Long Zhao, Jie Mei, Bin Shao, Wei Xiang, and Lajos Hanzo, "Survey of Large-Scale MIMO Systems", *Communications Surveys & Tutorials*, IEEE, 17(3):1738-1760, 2015.

[49] Fredrik Rusek, Daniel Persson, Buon Kiong Lau, Erik G Larsson, Thomas L Marzetta, Ove Edfors, and Fredrik Tufvesson, "Scaling up MIMO: Opportunities and challenges with very large arrays", *Signal Processing Magazine*, IEEE, 30(1):40-60, 2013.

[50] Berthold Panzner, Wolfgang Zirwas, Stefan Dierks, Mads Lauridsen, Preben Mogensen, Kari Pajukoski, and Deshan Miao, "Deployment and implementation strategies for massive mimo in 5G", *Globecom Workshops (GC Wkshps), 2014*, pages 346-351. IEEE, 2014.

[51] T. L. Marzetta, "Multi-cellular wireless with base stations employing unlimited numbers of antennas", *Proc. UCSD Inf. Theory Applicat. Workshop*, Feb. 2010.

[52] T. L. Marzetta, "Noncooperative cellular wireless with unlimited numbers of base station antennas", *IEEE Trans. Wireless Commun.*, vol. 9, no. 11, pp. 3590-3600, Nov. 2010.

[53] A. L. Swindlehurst, E. Ayanoglu, P. Heydari, and F. Capolino, "Millimeter-wave massive mimo: the next wireless revolution?", *IEEE Communications Magazine*, 52(9):56-62, September 2014.

[54] W. Roh, J. Y. Seol, J. Park, B. Lee, J. Lee, Y. Kim, J. Cho, K. Cheun, and F. Aryanfar, "Millimeter-wave beamforming as an enabling technology for 5G cellular communications: theoretical feasibility and prototype results", *EEE Communications Magazine*, 52(2):106-113, February 2014.

[55] J. Murdock *et al*, "A 38 GHz Cellular Outage Study for an Urban Outdoor Campus Environment", *Wireless Commun. Network. Conf.*, Apr. 2012, pp. 3085-90.

[56] T. Rappaport *et al*, "Broadband Millimeter-Wave Propagation Measurements and Models Using Adaptive-Beam Antennas for Outdoor Urban Cellular Communications", *IEEE Trans. Antennas and Propagation*, vol. 61, no. 4, pp. 1850-59, Apr. 2013.

[57] Korea, "Further Information on Technical Feasibility of IMT in the Bands above 6 GHz", *ITU-R WP5D - IMT Systems*, Contrib. 407, `http://www.itu.int/md/R12-WP5D-C-0407/en`

[58] H. Zhao *et al*, "28 GHz Millimeter Wave Cellular Communication Measurements for Reflection and Penetration Loss in and Around Buildings in New York City", *IEEE ICC 13*, pp. 516-67, June 2013.

[59] Y. Azar *et al*, "28 GHz Propagation Measurements for Outdoor Cellular Communications Using Steerable Beam Antennas in New York City", *IEEE ICC 13*, pp. 5143-47, June 2013.

[60] X. Huang, Y. J. Guo, and J. D. Bunton, "A hybrid adaptive antenna array", *IEEE Transactions on Wireless Communications*, 9(5):1770-1779, May 2010.

[61] A. Alkhateeb, J. Mo, N. Gonzalez-Prelcic, and R. W. Heath, "Mimo precoding and combining solutions for millimeter-wave systems", *IEEE Communications Magazine*, 52(12):122-131, December 2014.

[62] S. Han, C. l. I, Z. Xu, and C. Rowell, "Large-scale antenna systems with hybrid analog and digital beamforming for millimeter wave 5G", *IEEE Communications Magazine*, 53(1):186-194, January 2015.

[63] Jianhua Mo, Philip Schniter, Nuria Gonzalez Prelcic and Robert W. Heath, Jr. "Channel Estimation in Millimeter Wave MIMO Systems with One-Bit Quantization", Signals, Systems and Computers, 2014 48th Asilomar Conference, 2-5 Nov. 2014.

[64] Jiguang He, Taejoon Kim, Hadi Ghauch, Kunpeng Liu and Guangjian Wang "Millimeter Wave MIMO Channel Tracking Systems", [Available online at] `https://arxiv.org/pdf/1412.4224v1.pdf`.

[65] M. Akdeniz, M. S. Y. Liu, S. R. S. Sun, T. S. Rappaportand and E. Erkip, "Millimeter wave channel modeling and cellular capacity evaluation", [Available Online] `http://arxiv.org/abs/1312.4921`.

[66] S. Kirthiga and M. Jayakumar, "Performance and Capacity analysis of MIMO system at 5 GHz and 60GHz in Indoor Environment", *WSEAS Trans. on Commun.*, vol. 11, pp. 415-426, 2012.

[67] J. He, T. Kim, H. Ghauch, K. Liu and G. Wang, "Millimeter Wave MIMO Channel Tracking Systems", *Globecom 2014 Workshop - Mobile Communications in Higher Frequency Bands*, pp. 414-419, 2014.

[68] E. Torkildson, H. Zhang and U. Madhow, "Channel Modeling for Millimeter Wave MIMO", *IEEE Communications Magazine*, p. 1-8, 2010.

[69] R. Magueta, D. Castanheira, A. Silva, R. Dinis, A. Gameiro, "Linear Space-Time Equalizer for Single-User Hybrid mmWave Massive MIMO Systems", in *8th International Congress on Ultra Modern Telecommunications and Control Systems and Workshops*, Lisbon, Portugal, 2016.

[70] Meisam Khalil Arjmandi "5G Overview: Key Technologies", [Available online] `http://www.ittoday.info/Excerpts/5G-Overview-Key-Technologies.pdf`

[71] C. Wang, F. Haider, X. Gao, Y. Yang, D. Yuan, H. Aggoune, H. Haas, S. Fletcher, E. Hepsaydir "Cellular Architecture and Key Technologies for 5G Wireless Communication Networks", *IEEE Communications Magazine*, pp. 122-130, February 2014

[72] V. Jungnickel, K. Manolakis, W. Zirwas, B. Panzner, V. Braun, M. Lossow, M. Starnad, R Apelfrojd, and T. Svensson "The Role of Small Cells, Coordinated Multipoint, and Massive MIMO in 5G", *IEEE Communications Magazine*, pp. 44-51, May 2014.

[73] B. Bangerter, S. Talwar, R. Arefi, and K. Stewart, Intel "Networks and Devices for the 5G Era", *IEEE Communications Magazine*, pp. 90-96, February 2014.

[74] D. Neves, C. Ribeiro. A. Silva, A. Gameiro, "Channel estimation schemes for OFDM relay-assisted systems", in *proc. IEEE VTC spring*, 2009.

[75] C. Balanis *Antenna Theory*, Wiley, 1997.